Near-surface structures in the Cape Ghir filament off Morocco

Coastal upwelling
Filament
Northwest Africa
Water mass
Eddy

Upwelling côtier
Filament
Nord-ouest de l'Afrique
Masses d'eau
Tourbillon

Eberhard HAGEN [a], Christoph ZÜLICKE [b] and Rainer FEISTEL [a]

[a] Institut für Ostseeforschung Warnemünde (IOW), Seestrasse 15, D-18119 Warnemünde, Germany.

[b] Joint Research Centre, Institute for Remote Sensing Applications (IRSA), Marine Environment Unit, I-21020 Ispra (VA), Italy. (*Currently at the IOW.*)

Received 16/05/95, in revised form 18/01/96, accepted 23/01/96.

ABSTRACT

A meso-scale CTD survey was conducted off Cape Ghir (31° N) from 29 September to 3 October 1992, with the inspection of mass-field structures in the 300 dbar layer as its main objective, and relatively large tongue of cold surface water as the subject of investigation. This filament of upwelled water extends about 200 km seaward from the coastal zone of Morocco. Our CTD survey included two zonal transects 213 km in length, sampled synchronously by R/Vs *Hudson* along 31° 30′ N and *A. v.Humboldt* along 30° 30′ N. A meridional section followed the shelf edge at 10° 10′ W, and five zigzag sections were carried out above the Cape Ghir Plateau (CGP). Data resulting from an extended transect, sampled ten days earlier between 9° 43′ W and 14° W at 32° N, are also considered. Decadal means of available satellite IR data as well as bulk sea-surface temperatures (SST) indicate similar structures by a strict response of geostrophical motion patterns to irregularities in the bottom topography. The coastal jet bifurcates off the northern flank of the CGP. Its nearshore branch forms a cyclonic, eddy-like feature over the eastern part of the plateau. The related offshore branch feeds the filament with cold coastal water. The axis of that zonal filament follows the southern flank of the CGP at about 31° N. A simple balance of geostrophic net transports suggests that the mean upwelling velocity of the filament is of the same order within superficial layers as that of the coastal upwelling off Morocco. Two oppositely-rotating eddies interact to generate/maintain an intense seaward jet and to export cold upwelled water further out to sea, at least as far as 13° W.

RÉSUMÉ

Structures sub-superficielles dans le filament du cap Ghir au large du Maroc.

Une campagne hydrologique à moyenne échelle a été effectuée au large des côtes marocaines (cap Ghir, 31° N), du 29 septembre au 3 octobre 1992, en vue d'étudier la structure du champ de masse dans la couche de 300 dbar. L'extension d'une remontée d'eau froide a été suivie jusqu'à environ 200 km de la côte. Les données CTD ont été acquises sur : 1) deux radiales de 213 km parcourues simultanément par les navires océanographiques *Hudson* à 31° 30′ N et

A. v.Humbold à 30° 30′ N; 2) une section méridienne au bord du plateau continental à 10° 10′ W; 3) cinq sections en zigzags sur le plateau du cap Ghir (CGP), 4) le prolongement, entre 9° 43′ W et 14° W, d'une radiale suivie dix jours plus tôt à 32° N.
Les moyennes décennales de données satellitales IR et les températures superficielles globales (SST) indiquent des structures analogues dans les schémas de circulation géostrophique résultant des irrégularités de topographie du fond. Le jet côtier bifurque au large du flanc nord du plateau du cap Ghir; sa branche côtière forme une structure tourbillonnaire cyclonique à l'est du plateau; au large, la branche correspondante apporte au filament de l'eau côtière froide. L'axe de ce filament zonal suit le flanc sud du plateau vers 31° N. Un simple bilan des flux nets géostrophiques indique que la vitesse moyenne de l'upwelling du filament est du même ordre de grandeur dans les couches superficielles et dans l'upwelling côtier du Maroc. Deux tourbillons de sens opposés contribuent à former ou maintenir un jet intense qui entraîne l'eau froide vers le large, au moins jusqu'à 13° W.

Oceanologica Acta, 1996, **19**, 6, 577-598.

INTRODUCTION

In coastal upwelling areas, the surface temperature frontal zone often exhibits meanders with an alongshore scale that is similar to variations in the bottom topography (Ikeda *et al.*, 1984). It is a commonly accepted notion that the equatorward coastal/frontal jet is an ingredient of the large-scale upwelling process. This near-surface current follows the continental slope and advects water with upstream properties (Kosro *et al.*, 1991). Both the southward coastal jet and the along-slope frontal zone form a boundary for on-offshore motions. The boundary zone should be broken up over large alongshore distances to form filaments with intense mixing processes and eddy-like features which may break away from the boundary region (Smith, 1995). Filaments of upwelled water are frequently observed with a strict on-offshore orientation, especially in the vicinity of submarine plateaus and/ or canyons. A seaward jet is embedded in the large offshore meander of the near-surface frontal zone. According to Gabric *et al.* (1993) and Head *et al.* (1995), the associated cross-isobath flow is of some importance for the distribution of biological parameters. There is a clear identification of any "upwelling filament", in the form of relatively cold waters with low dissolved oxygen content but a pronounced enrichment of nutrients and – for instance – a higher biological productivity over strong irregularities in the continental slope. Due to topographic influence on the motion dynamics, the filament should be locally fixed. This hypothesis is supported by the predictions available from numerical models concerning the particular role of shelf plateaus and the associated response in the mass- and current-field under different forcing conditions (*cf.* Ikeda and Emery, 1984; Metzner and Hennings, 1990). On the other hand, we also find some observational evidence for the locally-fixed behaviour of resulting upwelling filaments (*cf.* Thomson and Emery, 1986; Lutjeharms and Stockton, 1987). A well-pronounced filament of coastal upwelling is found to be located over the Cape Ghir Plateau (31° N) off Morocco. This plateau is the submarine extension of the Atlas Chain on land. Such topographic structures act as barriers both to meridional winds and to currents. Up to now, we have lacked a detailed snapshot study describing the hydrographic structures in the context of remote sensing data on the sea-surface temperature (SST).

In order to elucidate characteristic filament conditions, the Institute for Remote Sensing Applications of the Joint Research Centre (Ispra, Italy), the Institute for Baltic Sea Research (Warnemünde, Germany), and the Biological Oceanography Division of the Bedford Institute of Oceanography (Dartmouth, Canada) carried out a joint field campaign with R/Vs *A. v.Humboldt* and *Hudson* over the Cape Ghir Plateau (CGP) during September/October, 1992. The main area under consideration is shown by a box together with rough topographic contours and a monthly averaged SST map in Figure 1. These values indicate the filament by SST < 20 °C. Results of hydrographic measurements carried out along 32° N in the northern part of our investigation area will be included in the following description.

Study Region

According to Isemer and Hasse (1987), the annual wind-stress curl indicates positive (cyclonic) values in the near-coastal zone but negative (anticyclonic) values further offshore in our study area. This structure causes current divergences in the oceanic top layer, especially along shelves, the resulting mass-deficit being mainly compensated by upwelling. Thus the Ekman vertical velocity is responsible for a large-scale cold water belt in the coastal zone (Brink, 1983). Resulting maps of the annually averaged vertical velocity indicate the order of 1×10^{-4} cm s^{-1} south of about 25° N. North of that latitude, this "steady-state" wind pattern is essentially modified by the meridional migration of the northeast trade wind during the seasonal cycle.

According to Wooster *et al.* (1976) and Speth and Köhne (1983), upwelling occurs at least south of about 34° N during summer and early autumn environmental conditions (July-October). With respect to the climatic conditions of the northeast trade, we note a paradoxical wind situation

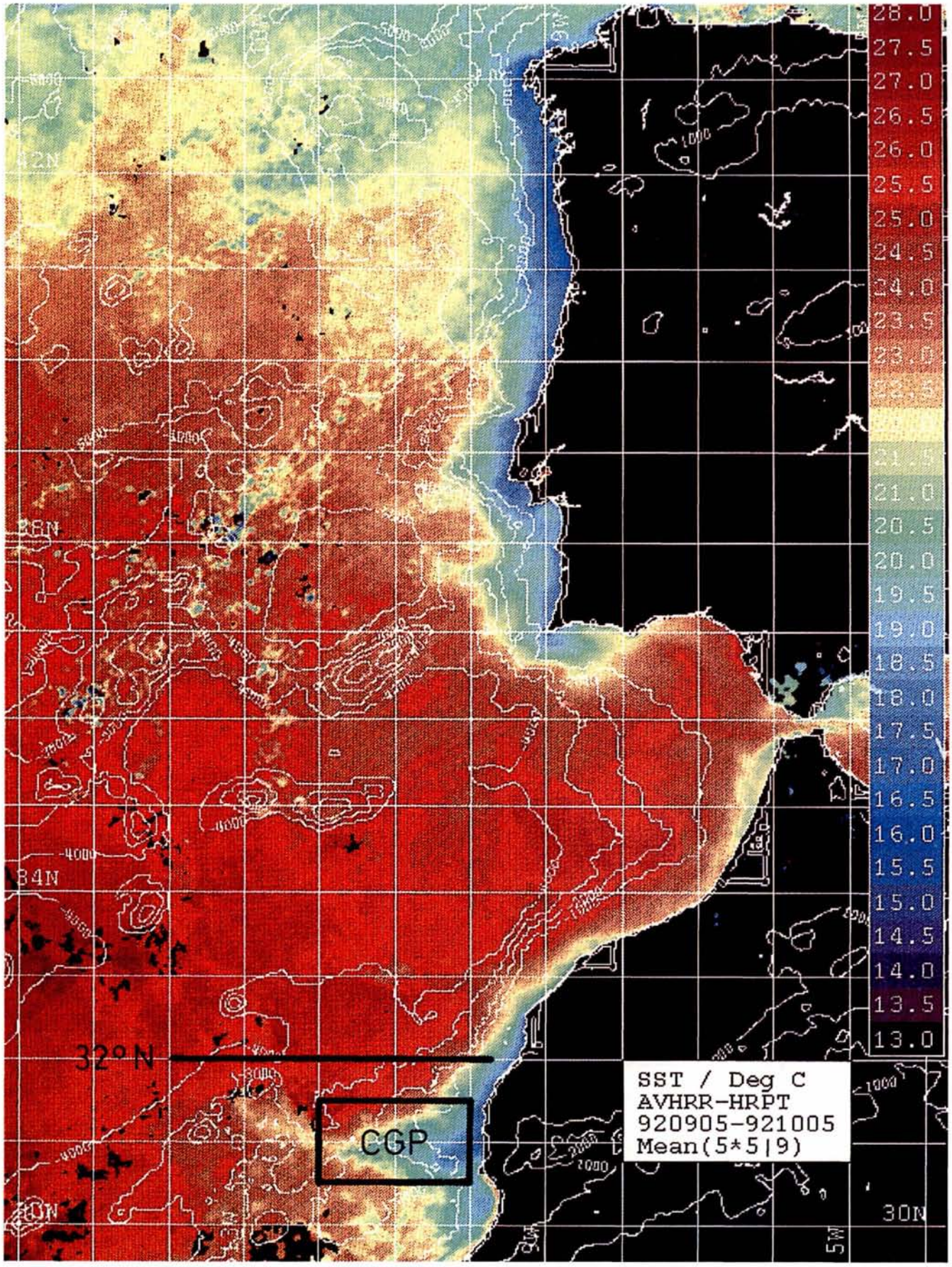

Figure 1

Rough contours of the bottom topography and orography in the northeast Atlantic Ocean; the monthly averaged SST-map (5 September - 5 October, 1992) is superimposed; a mean signal of coastal upwelling occurs off Portugal and Morocco; hydrographic measurements are carried out along the zonal section at 32° N (15-18 September, 1992) and within the box (29 September - 3 October, 1992) covering the extended cold-water filament above the Cape Ghir Plateau (CGP) at about 31° N; note that the plateau is the submarine extension of the Atlas Chain on land.

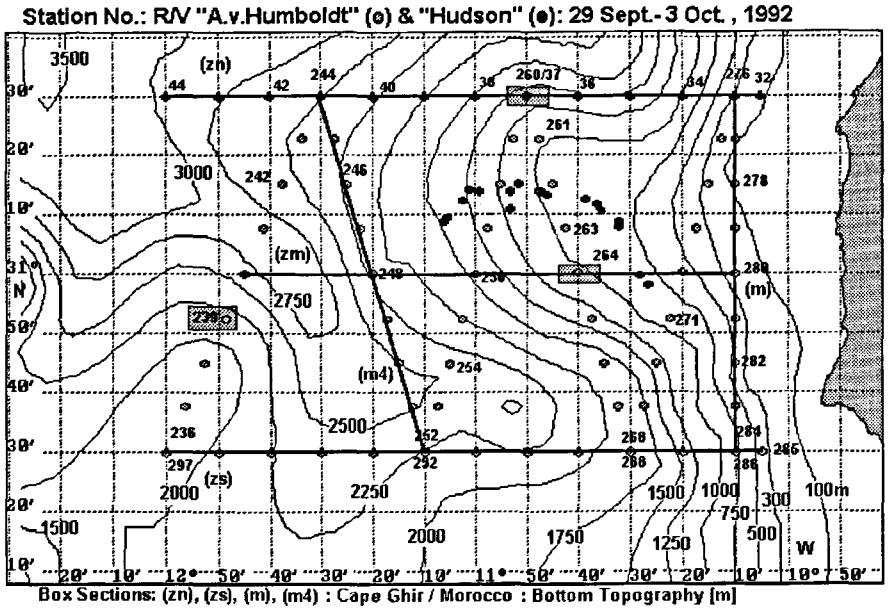

Figure 2

Joint grid of CTD-stations sampled between 29 September and 3 October, 1992, in the Cape Ghir upwelling filament; contours in the bottom topography are indicated by isobaths in metres; stations with full dots correspond to measurements by R/V Hudson *while stations with open circles were measured by R/V* A. v.Humboldt*; selected hydrographic sections (zn, zm, zs, m, m4) are given by bold lines; both zonal sections at 31° 30′ N (zn) and 30° 30′ N (zs) are simultaneously begun in the east and completed in the west.*

off Agadir, which could be based on the orographic influence of the Atlas Chain. North of 31° N, this chain acts as a barrier to southward-blowing winds. Meridional winds decrease with decreasing latitudes and/or change their sign, while the offshore component increases off Cape Ghir in summer. Completely different conditions occur during the winter season. The northeast trade is located to the south of the Atlas Chain. Upwelling favourable winds towards the south increase with decreasing latitude, at least to Cape Blanc (21° N). In the zone between 21° N and about 23° N, upwelling occurs throughout the year. Irrespective of the seasonal cycle in alongshore winds off Morocco, it seems that the Cape Ghir filament exists all year round, with a more or less pronounced SST signal.

To our knowledge, the first mention of the permanent existence of coastal upwelling patterns off Cape Ghir was made by Erimesco (1966). From his Table 5, we obtain single SST values for eight months. Assuming the annual cycle to be the dominant signal for the SST and using these data, collected between 1947 and 1979 by different research vessels, we can try to estimate the seasonal variation in the SST. The resulting curve is plotted in Figure 3 and suggests a semi-annual cycle, sea-surface temperatures showing relative maxima with about 17 °C in March, but also reaching about 18 °C in September/ October. The pronounced minimum of about 15-16 °C can be expected in April/May, a second minimum of about 16.5 °C occurring in January. These historical data also indicate differences of about –3 K between the Cape Ghir SSTs and those off Casablanca and Cape Barbas throughout the whole year and suggest permanent upwelling over the Cape Ghir Plateau (CGP).

The dynamics of wind-driven currents on the continental shelf is extensively discussed by Allen (1980). The alongshore wind component dominates the coastal upwelling. Time series of wind measurements from the coastal station of Agadir (30° 23′ N, 9° 34′ W) are analysed by Erimesco (1966) as well as by Kirk and Speth (1985). Pentad values of six-hourly mean values indicate weak velocities, which are lower than 3-5 m s^{-1}, throughout the year. Mean wind directions show southward components during the late autumn, winter, and spring but northward components during the summer and the earlier autumn. Nevertheless, it appears that the seasonal variation in the meridional component of coastal winds, as observed at Agadir, is related to the seasonal SST curve detected over the CGP. Although the local wind conditions can only generate a slight Ekman offshore transport, coastal upwelling occurs permanently. What could be the reason for this? There must be an additional forcing for the maintenance and/or generation of the "Cape Ghir Filament".

Field Studies

In the framework of the German contribution "Eastern Boundary Currents" (EBC) to the World Ocean Circulation Experiment (WOCE), CTD measurements were carried out along a zonal section at 32° N between 9° 43′ W and 14° W from 15 to 18 September, 1992, in order to study geostrophic current structures embedded in the EBC system (Hagen *et al.*, 1994). The station spacing was 15.7 km east of 10° 40′ W but 31.4 km further offshore. The resulting data are available from the WOCE data centre. Ten days later, our field campaign began in the region off Cape Ghir. The Cape Ghir Plateau (CGP), which occupies the region between 30° 30′- 31° 30′ N and 10°-12° W, obviously drastically deforms the meridional course of the continental slope. Station positions are shown above the rough bottom topography in Figure 2. The westward extension of isobaths marks the CGP and thus the submarine continuation of the Atlas Chain. The crest of this plateau starts at about 31° 10′ N, 10° 10′ W (300 m depth) in the near-coastal zone and shows an offshore extension to 31° 30′ N, 12° W (2750 m depth). A deep canyon-like channel occurs along its southern flank, reaching the continental slope with depths near 750 m in the vicinity of the position 30° 30′ N, 10° 15′ W.

Station positions are shown in Figure 2. Measurements were carried out from 29 September to 3 October 1992. The station spacing was 16 ± 0.5 km along the transects carried out by R/Vs *A. v.Humboldt* and *Hudson*. We began our observations with R/V *A. v.Humboldt* at station 236 and finished at station 297, at the same westernmost position of the southern zonal section. All station numbers lower than 60 were surveyed by R/Vs *Hudson*. Both research vessels synchronously sampled stations along two zonal sections at 31° 30′ N and 30° 30′ N on 3 October, 1992. Their offshore extension was 213 km, with the starting point at 10° 05′ W over the shelf. Thereafter, R/V *Hudson* followed free-drifting biological traps along a banana-like path, while R/V *A. v.Humboldt* carried out five zigzag sections and one meridional section along the shelf edge between the 300 m and 600 m isobaths.

The measurements are based on conductivity (C), temperature (T), pressure (P), depth (D), and dissolved oxygen (O_2) profiles using the CTD probe OM-87 on board R/V *A. v.Humboldt*, which is described by Möckel (1980), and a Seabird system on board R/V *Hudson*. The underwater unit was lowered from the sea surface down to 30 Bar (300 m), the maximum depth being the greatest accessible to the fluorometers mounted on the CTD probes. It has, however, been suggested on the basis of current-meter data in Rienecker and Mooers (1988) that the upper ocean variability in coastal upwelling areas may be usefully analysed without a full knowledge of the deeper flow.

The temperature sensor of the OM-87 probe was always controlled by three reversing thermometers at each station at the different horizons selected. For example, the mean sampling error of the temperature sensors of the CTD probe used on board R/V *A. v.Humboldt* was ± 0.02 K. In fact, that value reflects a poor quality for standard CTD temperatures. However, we lost our own CTD probe in the Gulf of Cadiz during that cruise. Temporal shifts of the electronic characteristics could be only partly corrected for the reserve probe. Comparisons were also carried out for salinity by salinometer measurements and for dissolved oxygen by the Winkler method. Resulting uncertainties were ± 0.047 (practical salinity unit) for salinity and ± 0.32 ml l^{-1} for dissolved oxygen. Our values must be multiplied by 44.66 in order to convert them from measurements in millilitres per litre (ml l^{-1}) to micromoles of dissolved oxygen per cubic decimetre of water at 20 °C (UNESCO, 1987*a*).

Using the UNESCO formulas for the equation of state (UNESCO, 1987*b*), the density was calculated from (S,T,P) values after the procedure of data validation in pressure steps of 5 dbar. The reference level for both the potential temperature and the potential density (PD) was always selected to be at the sea surface. We merged both hydrographic data sets although those obtained by R/V *Hudson* do not provide continuous profiles of dissolved oxygen. For example, Figure 4 shows T-S plots measured by different CTD probes at the same position but with a time lag of one day. The station position is separately depicted in Figure 2. Both curves coincide well for $T < 16.5$ °C and $S < 36.4$ from layers deeper than 70-170 m. This depth depends on the offshore distance. For a fixed salinity, both plots are shifted to lower temperatures with respect to the straight line of the North Atlantic Central Water (NACW). Discrepancies only occur in the near-surface layer due to actual mixing processes starting at the sea surface.

Satellite-derived SST images were processed on the basis of infrared (IR) soundings from space. The data were measured by the Advanced Very-High Resolution Radiometer (AVHRR) on the polar-orbiting satellite NOAA-11 in five different channels. After geo-referencing and cloud-masking of the single scenes, Multi-Channel SST (MCSST) maps were produced using the software package "TeraScan" according to Zülicke (1994*a*). These data were compared with reference skin-SST measurements and were found to be accurate to within 0.1 ± 0.4 K, Zülicke (1994*b*). Such values lie in the usual range (Schlüssel *et al.*, 1987).

Sea-Surface Structures

Many SST maps provided by satellites show the Cape Ghir filament as a cold-water tongue, extending offshore to a

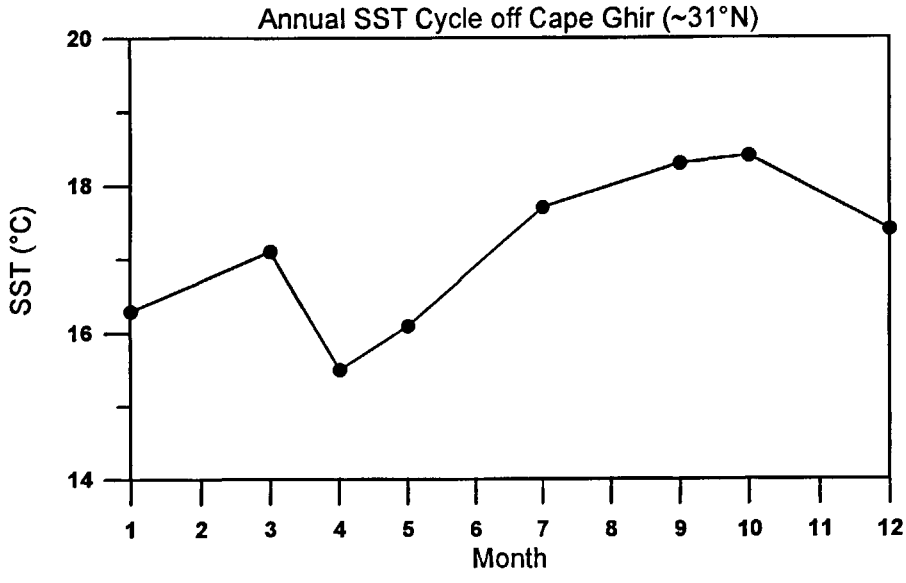

Figure 3

Composed seasonal cycle of the sea-surface temperature (SST) off Cape Ghir from data of Table 5 in Erimesco (1966).

distance of about 150 km at 31° N, *cf.* Nykjaer *et al.* (1987). Visually, the filament axis zonally follows the southern flank of the CGP up to about 12° W in Figure 5*a*, *c*. Averages from the period 5-15 September, 1992, just before our field campaign started, are mapped in Figure 5*a*. Hydrographic measurements were carried out along 32° N during 15-18 September. The corresponding SST map shows the coastal cold-water belt inshore of the 500 m isobath in Figure 5*b*. Over the CGP, the cold-water filament extends further offshore, at least up to 11.5° W. The SST map of Figure 5*c* covers the period 25 September-5 October. This period includes our field campaign, which was carried out above the CGP from 29 September to 3 October. Again, the most pronounced upwelling signal is located near 31° N. The westward extension of the associated filament (SST < 19 °C) can be identified up to 11° 40′ W with an offshore distance of about 300 km at 30° 50′ N. Further offshore (13° W), the filament signal disappears. A comparison of all three SST maps in time shows that the upwelling processes decrease in the northern and southern shelf areas. For instance, the offshore position of the 19 °C – isotherm is much smaller not only at 32° N but also at 30° N at the beginning of October than earlier in September, roughly by a factor of 2. Simultaneously, the meridional extension of the wedge-shaped filament significantly decreases along 11° W. However, the zonal extension of the filament axis shows no significant reduction along 30° 50′ N. This fact suggests that the offshore export of cold water is "at all events" maintained while the Ekman offshore transport weakens in neighbouring shelf zones. Furthermore we may conclude that our main field campaign took place during a relaxation period in the large-scale upwelling process.

Arrows of station winds are drawn in Figure 6. Wind directions change between NW, N, and NE with dominating winds from NNE. Temporal and spatial averages indicate a main direction of 15° from North with a velocity of 6.1 m s^{-1}. In general, we note relatively homogeneous wind directions with changing velocities in the range 1-10 m s^{-1}.

The CTD profiles provide bulk SST (T), sea-surface salinity SSS (S), and dissolved oxygen (O_2) from depths between 0.5 m and 1.5 m. Resulting structures are mapped with those of the potential density (PD) in Figure 7*a*, *d*. The SST distribution is plotted in Figure 7*a*. Its pattern confirms the cold-water structure of Figure 5*c*. For instance, the course of the 20 °C-isotherm roughly marks the position of the near-surface frontal zone separating the cold upwelling waters from warm offshore waters. The SST distribution visually indicates a strong correspondence to contours in the local bathymetry. It appears that the course of the 20 °C isotherm follows the 1500 m isobath, however, with a slight southward displacement. For example, the detected cold-water centre (T = 17.5 °C at 31° N, 10° 20′ W) shows a southward displacement of about 40 km from the crest of the plateau. This pattern takes place above the southern flank of the CGP. Its relative minimum (SST < 18 °C) marks the actual upwelling centre above the shelf edge. A thermal front zone is indicated by sharp lateral gradients northern of 31° N. This frontal zone changes its direction from northeast to southwest and separates warm offshore water (SST > 20 °C) from wind-mixed upwelled water (SST < 19 °C). The frontal zone is also revealed by relatively strong gradients (in the SSS, Fig. 7*b*). Saline near-surface water (SSS ≥ 36.6) is visible in the northwest, while "fresher water" (SSS ≤ 36.3) occurs in the southwest. Usually, an actual upwelling plume is characterized by relative minima of both SST and SSS. The active upwelling centre (SSS < 36.1) is located on the shelf in the northeast corner. The shape of the frontal zone suggests a cyclonic, eddy-like feature over the CGP, while the zonal axis of the filament coincides with the latitude of 30° 50′ N. The discussed structures relating to both SST and SSS determine the near-surface distribution of the potential density (PD), which is mapped in Figure 7*c*. Large values indicate upwelled cold water, while a small spacing of isopycnals reveals the large meander of the frontal zone. The frontal jet follows the cyclonic curvature of the frontal system. The smaller the spacing, the greater the core speed of embedded

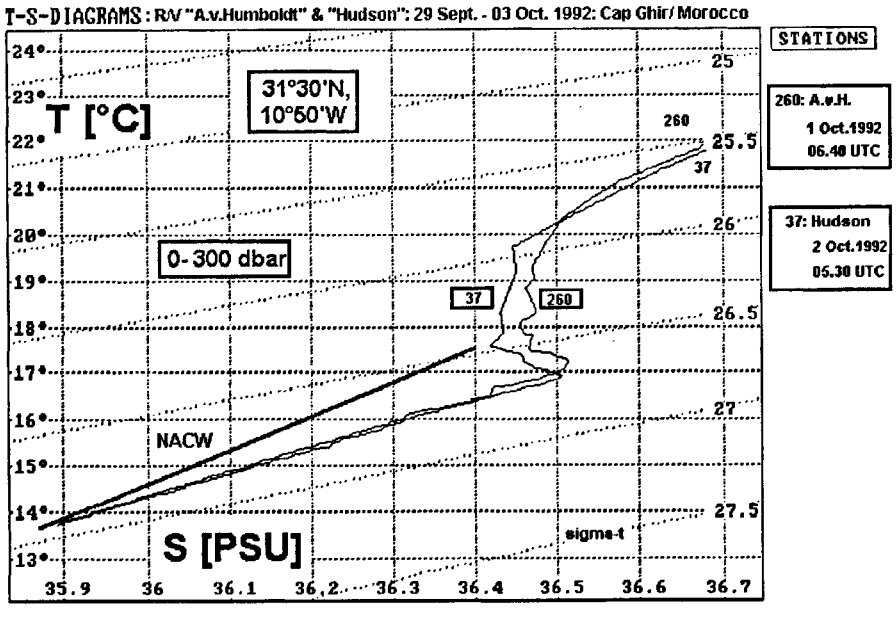

Figure 4

Temperature (T)- salinity (S) plots as mesured by different CTD probes used on board R/Vs Hudson *(station 37) and* A. v.Humboldt *(station 260) at the same position but with a lag of about one day; the straight line describes properties of the North Atlantic Central Water (NACW), cf. Figure 2 for the station position; the salinity is given as practical salinity units (PSU).*

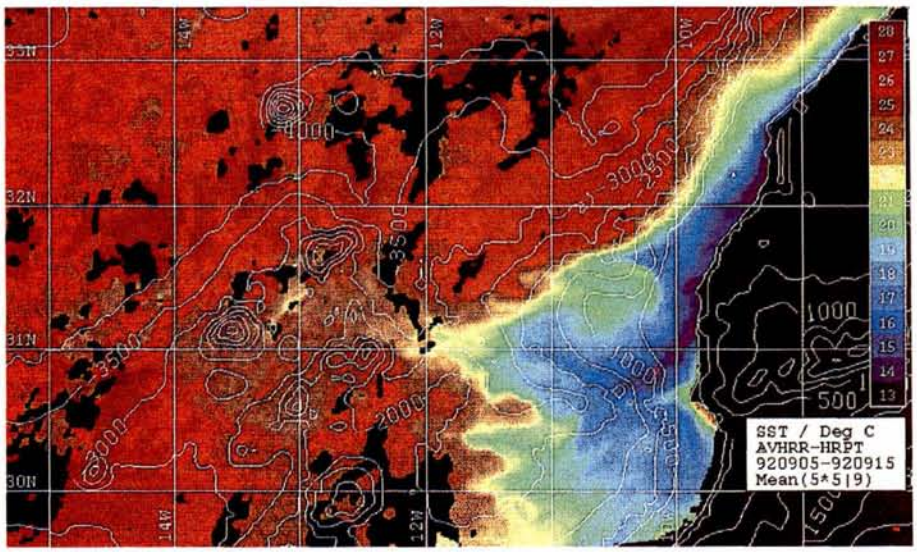

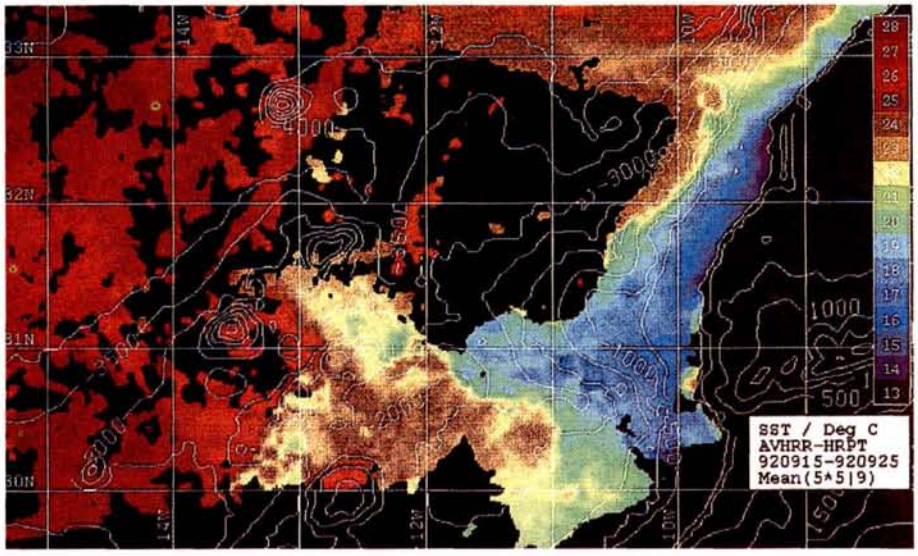

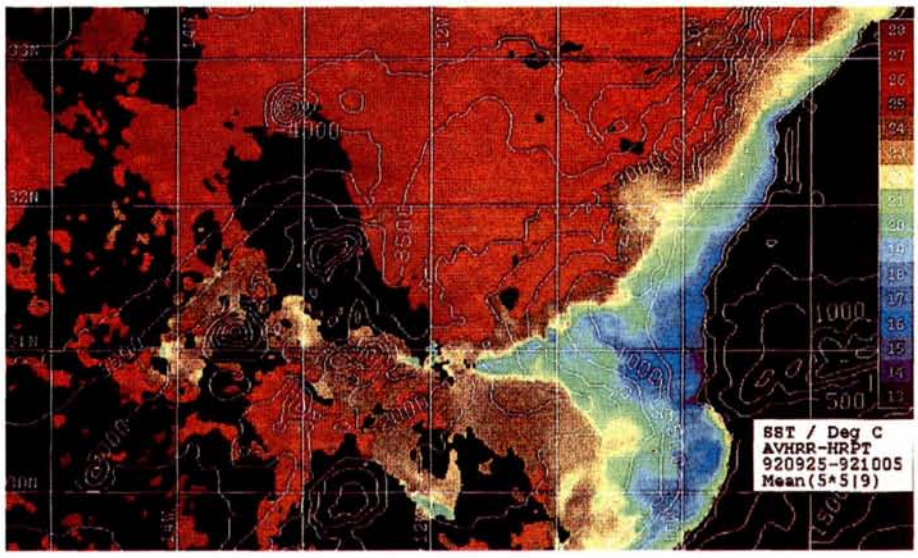

Figure 5

Decadal means in the mapped sea-surface temperature in comparison with the rough bottom topography for three stages:
a) 5 to 15 September, mapping the ten-day period before the joint field campaign.
b) 15 to 25 September, covering observations along the zonal section at 32 N (15-18 September).
c) 25 September to 5 October, describing the averaged conditions during the hydrographic measurements off Cape Ghir (29 September-3 October).

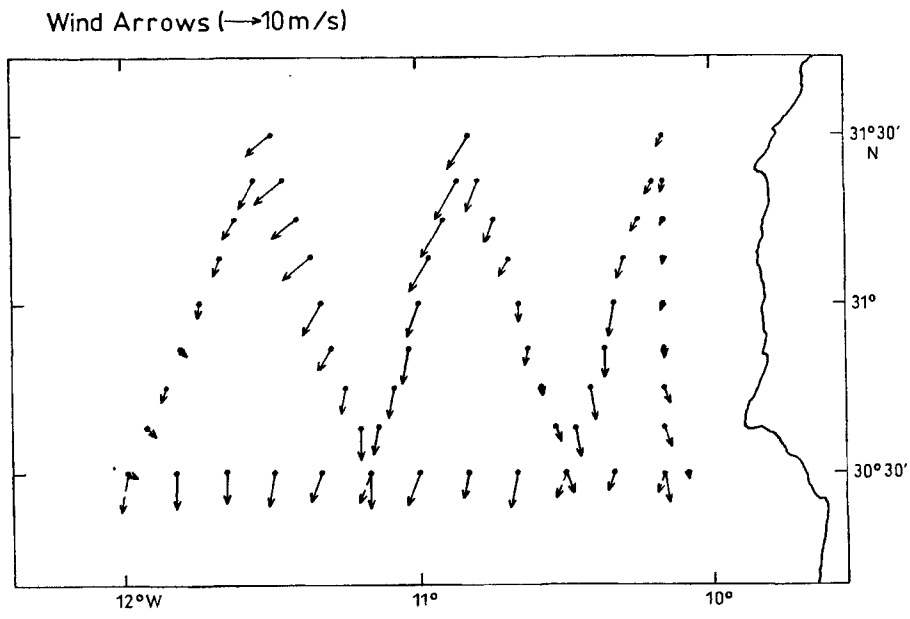

Figure 6

Wind arrows from station observations carried out by R/V A. v.Humboldt *between 29 September and 3 October, 1992; ship's track is described in the text.*

geostrophic currents headed southward with higher densities on their cold-water side. The distribution of dissolved oxygen is plotted in Figure 7*d*. The course of the 4.8 ml l^{-1}-value coincides with that of the frontal zone and separates the well ventilated coastal water ($O_2 > 5$ ml l^{-1}) from the offshore water ($O_2 < 4.6$ ml l^{-1}) zonally.

In summary, maps of skin-SSTs and bulk SSTs are highly correlated and point to the existence of a sharp frontal zone, which is also visible in SSSs and in the oxygen distribution. Corresponding density patterns suggest an embedded geostrophic coastal jet flowing southward within a large cyclonic meander over the CGP. The frontal jet reaches its westernmost position at 30° 50′ N. The related filament axis could be identified along the southern flank of the CGP. There would appear to be a dynamic response of upper layer currents to deeper motions, which are influenced by the CGP.

Water Masses

The properties of water masses can be well described by T-S / T-O_2 diagrams. Both T and S are highly conservative, while dissolved oxygen is also influenced by biological dynamics. Plotting all vertical T-S profiles together, a high degree of near-surface variability is evident (Fig. 8*a*). Its temperature range covers values T > 16 °C, while the corresponding salinity lies between 36.1 and 36.7. The T-O_2 plots indicate a relative maximum of about 5.2 ml l^{-1} for temperatures between 16.5 °C and 19 °C in Figure 8*b*. Comparison of that temperature range in Figure 16*a* with the vertical density distribution in Figure 16*c* reveals that the enrichment of dissolved oxygen occurs beneath the pycnocline at depths between 70 m and 120 m. The averaged content of oxygen is only 0.5 ml l^{-1} lower in intermediate layers near 300 m depth than in the surface layers. Generally, the actual pycnocline is roughly bounded by the 17°-19 °C isotherms. Thus, the near-surface layer is separated from intermediate layers at about 60 dbar (60 m). For T < 16 °C (depths greater than 100-120 m), the influence of the near-surface variability disappears and a straight line occurs in the T-S relationship. This line corresponds to conservative properties of the North Atlantic Central Water (NACW), with limits tabulated in Table 1.

Two salinity regimes occur for T < 14 °C. Such structures could be caused by a spatial separation of intermediate water masses. There are three possible sources for such water properties:

- Upper level NACW;
- Mediterranean Water with a higher degree in salinity but poor in dissolved oxygen;
- 18 °C-mode water with higher values in dissolved oxygen but low salinity.

According to Siedler *et al.* (1987), the 18 °C-mode water (Madeira mode water) is seasonally formed by winter convection. In order to clarify the situation, we return to the near-surface structures in the SST distribution. The course of the surface frontal zone is well indicated by the 20 °C isotherm. Roughly, SST < 20 °C correspond to the region with cold coastal water. The T-S diagrams of selected stations with SST < 19.5 °C are plotted in Figure 9. Here, only one straight T-S relationship is visible for T < 14.5 °C and S < 36.1. Characteristics of the pure NACW only occur with T < 13.5 °C and S < 35.9 at depths of about 300 m. Within the salinity regime between 35.9 < S < 36.1, the measured temperature is somewhat lower than that of the NACW, about 0.2-0.5 K. We conclude that the

Table 1

Temperature (T) and salinity (S) values for the upper and lower limit of the North Atlantic Central Water (NACW) according to Willenbrink (1982)

NACW	Upper Limit	Lower Limit
T / °C	17.5	8.0
S	36.4	35.1

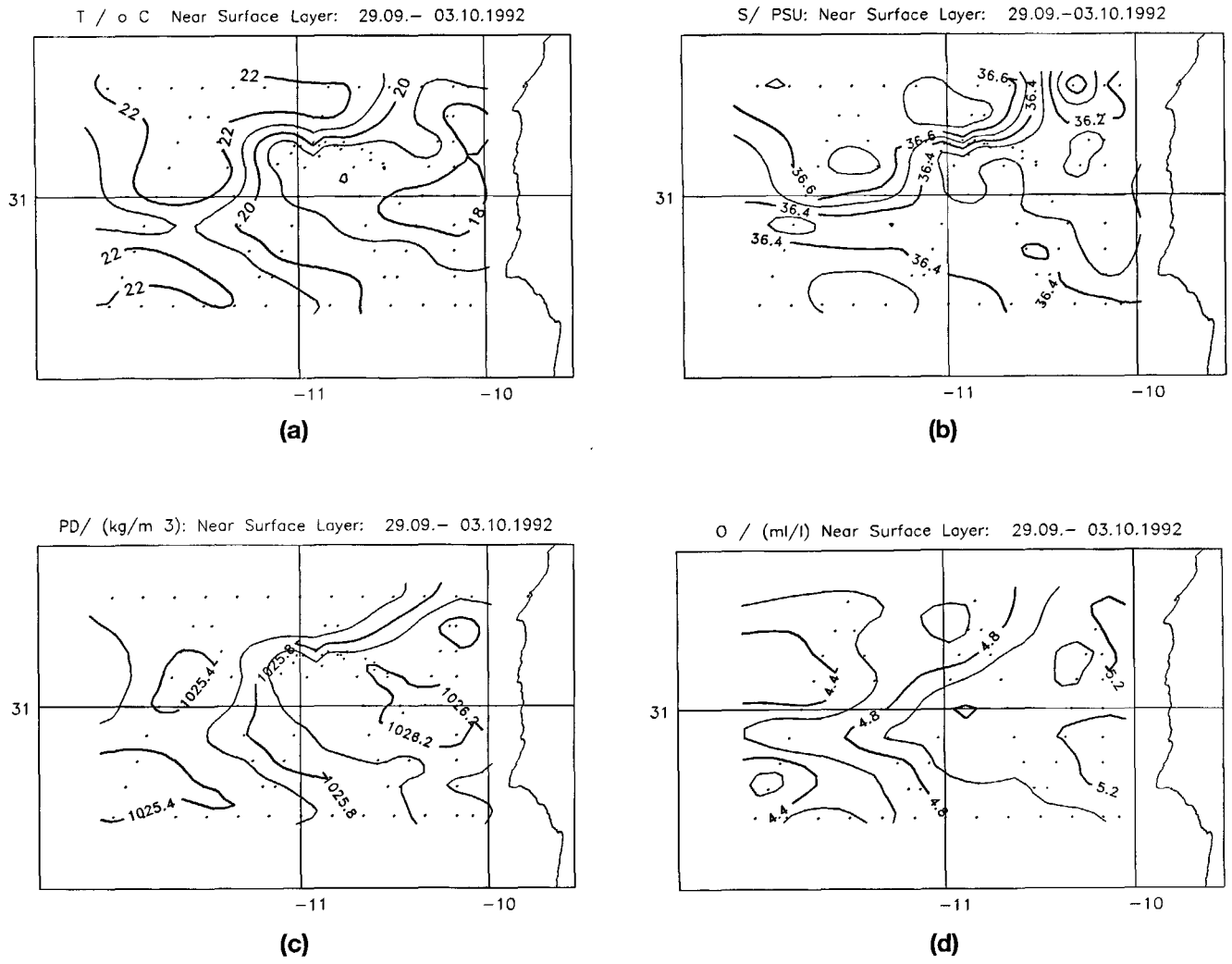

Figure 7

Hydrographic conditions within the near surface layer as obtained from CTD measurements down to depths of about 5 m: a) temperature (T), ΔT=1 K; b) salinity (S), ΔS = 0.1; c) potential density (PD), ΔPD = 0.2 kg m^{-3}; d) dissolved oxygen (O_2), ΔO_2 = 0.2 ml l^{-1}

intermediate inflow of warmer water only takes place at some stations in the offshore region characterized by SST > 20 °C, probably along the near-surface frontal zone. Up to now, it has appeared that the southward frontal jet influences the whole 300 m layer and advects T-S properties of relative warm and saline water from the North into the region of the Cape Ghir filament. Where does this current come from?

Transect at 32° N

In order to elucidate the origin of the southward-moving coastal jet, we may inspect measurements carried out along an extended zonal section at 32° N, ten days before the hydrographic survey was carried out off Cape Ghir.

The measurements started at station 168 (14° W) and ended with station 184 (9° 43′ W). The observations of station winds are plotted in Figure 10. We are looking to the west along this section. Between the easternmost station 184 and station 180 (10° 20′ W), constant wind directions from 30°-40° (NNE) confirm the northeast trade with velocities between 9 m s^{-1} and 10 m s^{-1}. Peak values are observed at station 179 (10° 30′ W). The wind velocity clearly increases up to 14 m s^{-1} while the wind direction clockwise rotates by 10°-20° from station 180 to station 179. This looks like a discontinuity in local winds, an atmospheric frontal zone. Corresponding structures in the air-pressure distribution confirm that conclusion for the zone between stations 180 and 175 (11° 40′ W). Its zonal width is about 110 km. The strongest zonal gradient occurs between station 178 (10° 40′ W) with 1015.5 hPa and station 180 with 1014.0 hPa. This gradient suggests a maximum in southward-blowing geostrophic winds at station 179. Seaward of station 179, the wind velocity permanently decreases down to 6 m s^{-1} while its direction continuously rotates anticlockwise from NE to N to NW. On the basis of our data, we cannot determine whether this atmospheric front is a permanent feature, which could be based on the coastal upwelling belt, or a transient phenomenon. Near-surface wind observations resulting from two buoys and one coastal station suggest the existence of a permanent atmospheric frontal zone off Cape Blanc (21° N) (Halpern and Stuart, 1975). Its offshore distance of about 130 km is

associated with the daily wind cycle. Such an atmospheric frontal zone separates the cold air regime of the coastal upwelling belt from the warm air regime further offshore.

Zonal temperature and salinity distributions at the pressure level of 30 dbar are plotted in Figure 11. Relatively constant temperatures of about 22.2 °C occur seaward of station 176 (11° 20′ W), while the upper-layer temperature rapidly increases with decreasing section distance to the east of station 180 (10° 20′ W). The lowest value of 15.5 °C indicates quite active coastal upwelling at the easternmost station 184 (9° 43′ W), which lies at 47 m water depth on the shelf. Here, the lowest salinity value of 36.1 was measured.

Between stations 184 and 180, the zonal gradients in T and S show a similar tendency, with minimum values in the east. An oceanic frontal zone must also be located in the vicinity of station 180, which separates the coastal upwelling zone from the offshore region in near-surface layers. This front zone lies somewhat to the east of the atmospheric front zone. Relative peak values, in both temperature and salinity, are measured at station 180. This station is located 16 km east of the observed peak values both in wind direction and speed at station 179. Seaward, the near-surface frontal zone T decreases, but S increases up to station 176 while both parameters increase further offshore. On the basis of our available data, we are, however, unable to show a dynamic/kinematic link between the atmospheric and oceanic frontal zones.

We calculated the geostrophic meridional currents relative to the depth of about 1200 m following the proposal by Fiekas *et al.* (1992). Methodological uncertainties related to the accuracy of the CTD probe lie in the range ± 3 cm s^{-1}. For comparability, we zoomed out the upper 300 m layer in Figure 12. The following may be noted:

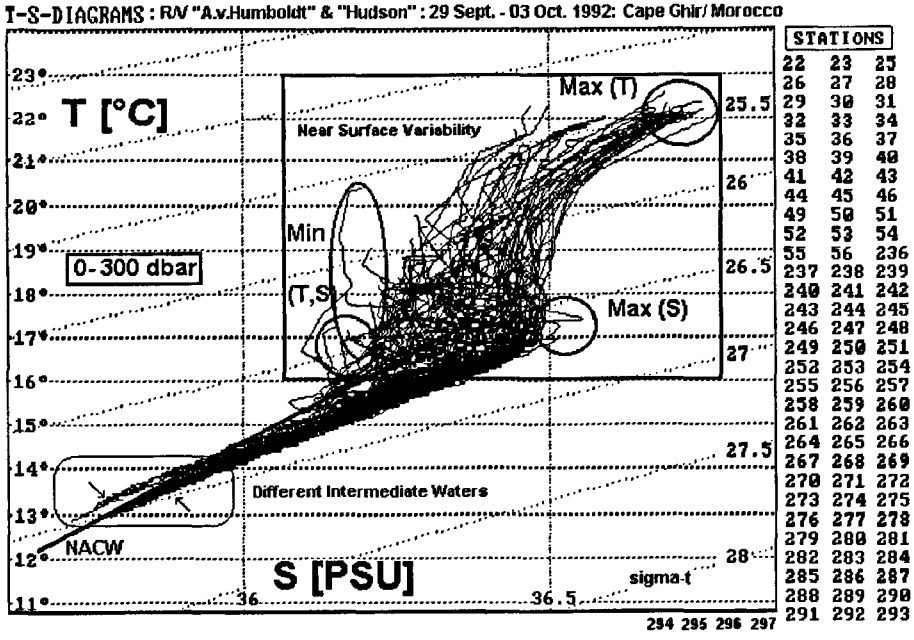

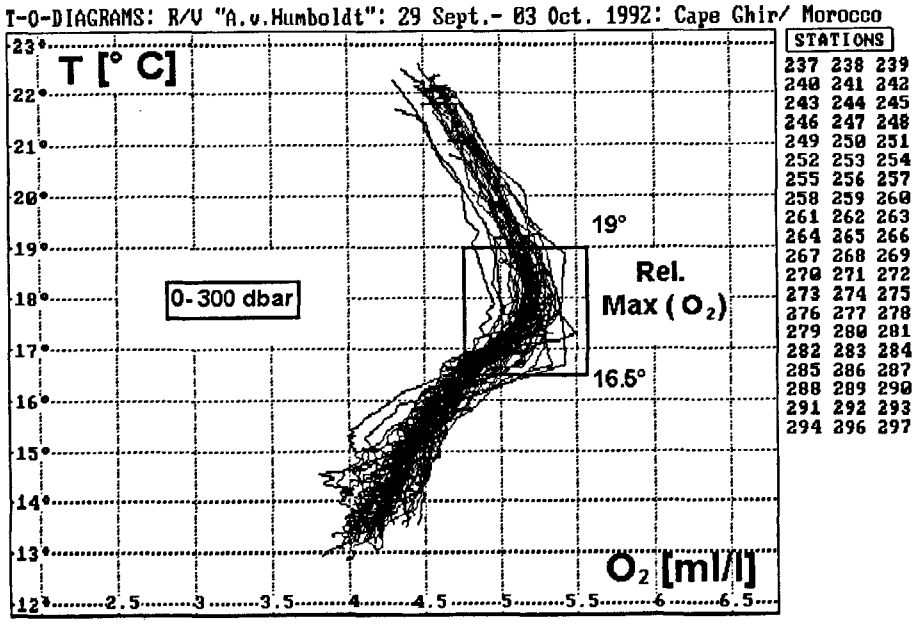

Figure 8

Scatter diagrams of temperature (T):
a) With salinity (S) indicating relative peak values within intermediate layers; the near-surface variability acts down to the depth of the isotherm of 16 °C (60-200 m), properties of the North Atlantic Central Water (NACW) are indicated by a straight line; two "bunches" suggest the existence of different intermediate waters beneath the isotherm of 14 °C (210-300 m); station positions are mapped in Figure 2.
b) With dissolved oxygen (O_2) revealing a pronounced maximum in the temperature range (16.5 < T < 19) °C, station positions used are shown in Figure 6.

Figure 9

T-S diagrams from all stations with relative cold water at the sea surface 17 < SST < 19.5 °C; the straight line corresponds to NACW; the near-surface variability acts down to the depth of the isotherm of about 15 °C (140-240 m); below 15 °C only one intermediate water mass occurs with a linear T-S relationship.

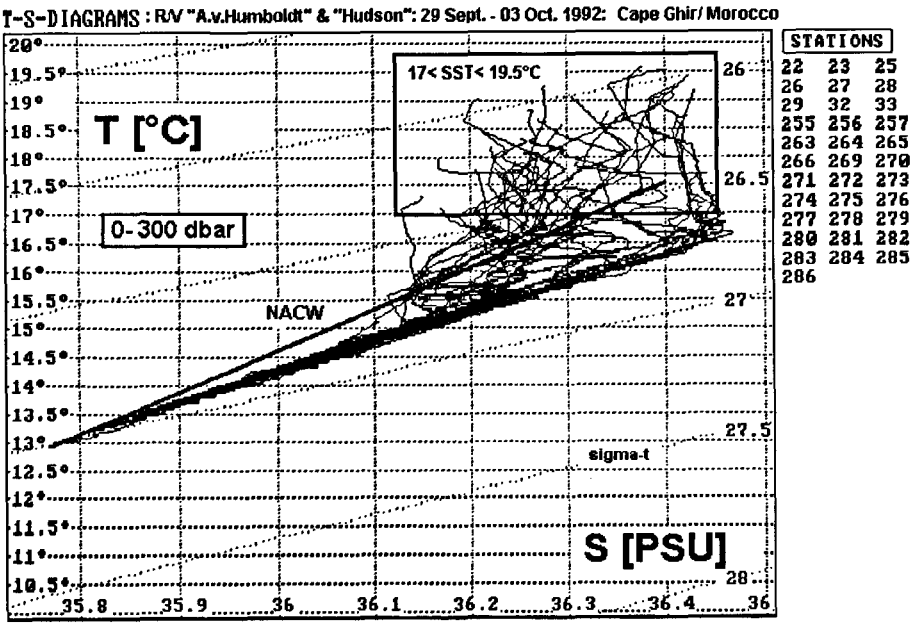

– In the eastern section distance of 150 km, two pronounced current cores occur between stations 184 and 176 within the 100 m-top layer .

– Offshore scale coincides with the offshore extension of the atmospheric frontal zone.

– Both geostrophic current cores show similar velocities near 15 cm s^{-1} but an opposite direction.

– The strongest current shear zonally occurs between stations 178 (10° 40′ W) and 179 (10° 30′ W), where the axis of the atmospheric frontal zone could be identified. Here, the north-bound current in the west is separated from the south-bound current above the continental slope in the east.

– The core of the south-bound current is placed at station 180 (10° 20' W), where the oceanic near-surface frontal zone was observed. The corresponding core speed is bounded by the isotache of –13 cm s^{-1} down to about 50 m depth. The isotache of 4 cm s^{-1} marks the vertical current extension down to about 100 m. The location of the current core coincides with that of relative peak values both in T and in S at the pressure level of 30 dbar.

– The deeper part of the southward-flowing coastal jet, which is embedded in the near-surface frontal zone, transports warm and saline waters in a seaward direction off Cape Ghir.

This last conclusion is well supported by the comparison of three T-S-plots in Figure 13. We selected:

– Station 180, which could be identified with the core position of the southward-flowing coastal jet at 32° N.

– Station 239, which lies in the path of the jet meander but in the southwestern corner of our investigation area.

– Station 264, which should be representative for the cold water filament conditions above the southern flank of the CGP.

The positions of the last two stations are separately stressed in Figure 2 while that of the first is given, for example, in Figure 12. T-S-plots of stations 180 and 239 coincide for T < 15.3 °C and S < 36.1. These values indicate water depths deeper than about 200 m. Consequently, the "intermediate warm water intrusion" indicated in Figure 8*a*, could be the consequence of water properties transported downstream by the deep branch of the southward going frontal jet meandering above the CGP. Consequently, the source of its T-S-characteristics must be sought to the north of 32° N.

Geostrophic currents

To describe the vertically-integrated flow field in the 50-150 dbar superficial layer, we computed the relative dynamic topography at 50 dbar relative to the reference level at 150 dbar. Such a map describes spatial anomalies in the potential energy resulting from differences in the mass-field. Corresponding isolines can be interpreted in the manner of geostrophic streamlines. Resulting structures are plotted in Figure 14*a*. The smaller the distance between neighbouring isolines, the stronger the geostrophic motion with high topographic values on its right-hand side. Resulting patterns will be, for instance, compared with those of dissolved oxygen drawn at the pressure level of 150 dbar in Figure 14*b*. Both panels show a general similarity by their isolines. We note the following:

– Off the northern flank of the CGP, the geostrophic southward current acts down to about 150 m depth. Its core bifurcates into two branches: a westward branch with anticyclonic curvature; and a southward branch with cyclonic curvature.

– The southward branch constitutes the true coastal jet and follows the shelf edge, but crosses the plateau at about 10° 20' W over water depths between 300 m and 750 m. This geostrophic jet meanders cyclonally above the CGP and follows the near-surface frontal zone separating the upwelled water, which is relatively poor in oxygen, from somewhat better ventilated offshore water.

– Two eddy-like features are perceived in the semi-closed isoline of –2.6 m^2 s^{-2} in the northwest corner and that of –2.66 m^2 s^{-2} in the southwest corner of our area.

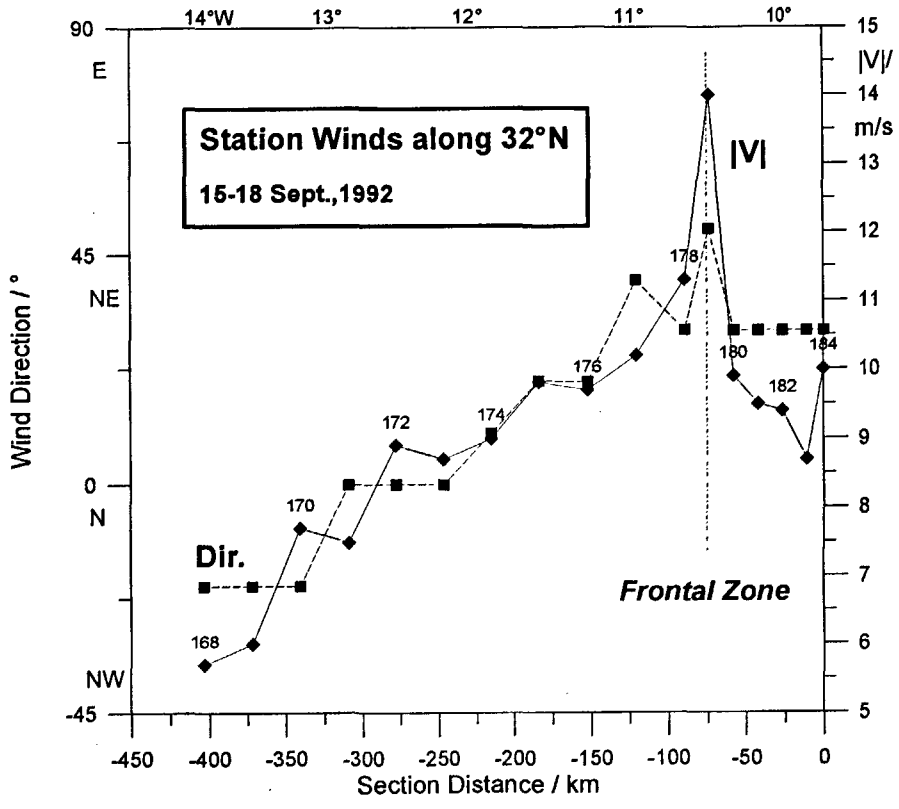

Figure 10

Wind direction (dotted line) and wind velocity [V] (heavy line) with station numbers along the zonal section at 32° N; peak values show the position of an atmospheric frontal zone separating the near coastal belt from the offshore regime at 10° 30' W; the location of the section is shown in Figure 1.

– The cyclonic feature takes place over the southwestern flank of the CGP and is associated with poor dissolved oxygen (< 4.3 ml l^{-1}) at 150 dbar, due to locally intensified upwelling.

– The anticyclonic feature is related to the westward current branch and takes place over the northwestern flank of the CGP. Here, downwelling provides that superficial layer with well-ventilated near-surface water (> 4.8 ml l^{-1}).

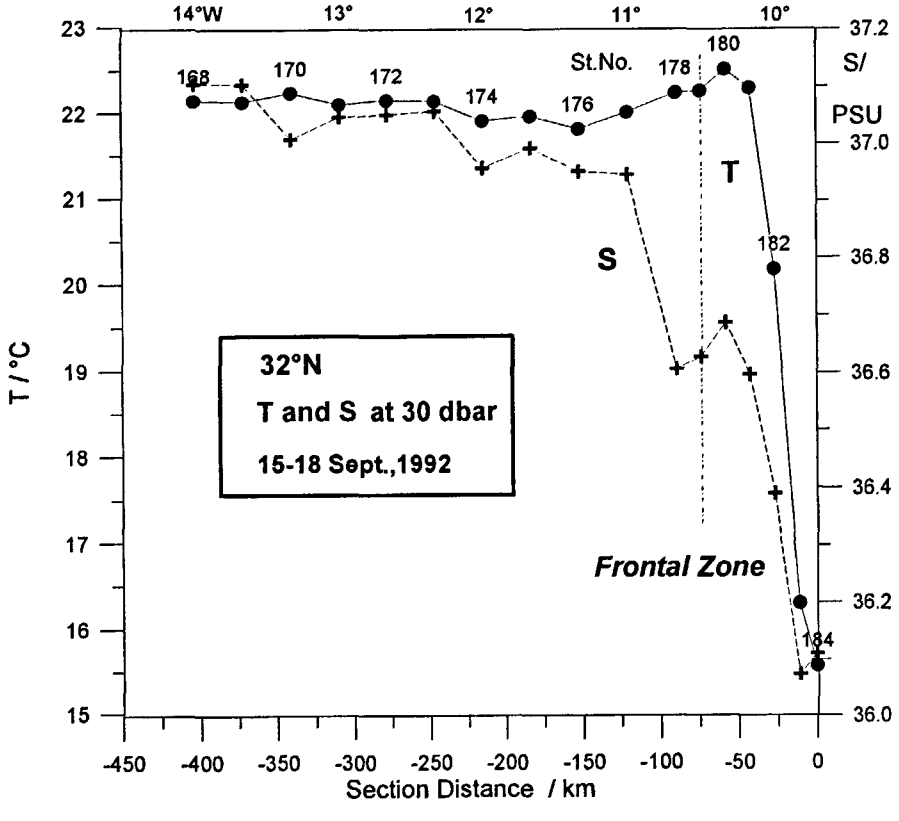

Figure 11

Zonal distribution in temperature (T) (full line with labelled station numbers) and salinity (S) (dashed line) at the pressure level of 30 dbar along the section at 32° N; the position of the meteorological frontal zone shown in Figure 10 is indicated by a thin vertical line; strong zonal gradients both in T and in S mark the oceanic frontal zone in the east of the atmospheric front with relative peak values at station 180.

Figure 12

Geostrophic meridional currents in the upper 300 m layer (30 Bar) using the reference level proposed by Fiekas et al. *(1992); positive values indicate northward currents (N) while negative values show southward currents (S); note the southward current core of –13 cm s^{-1} at station 180 where the slight peak values in T and S are revealed in Figure 11; in a zonal distance of about 50 km this current transports relatively warm and saline water in the downstream direction.*

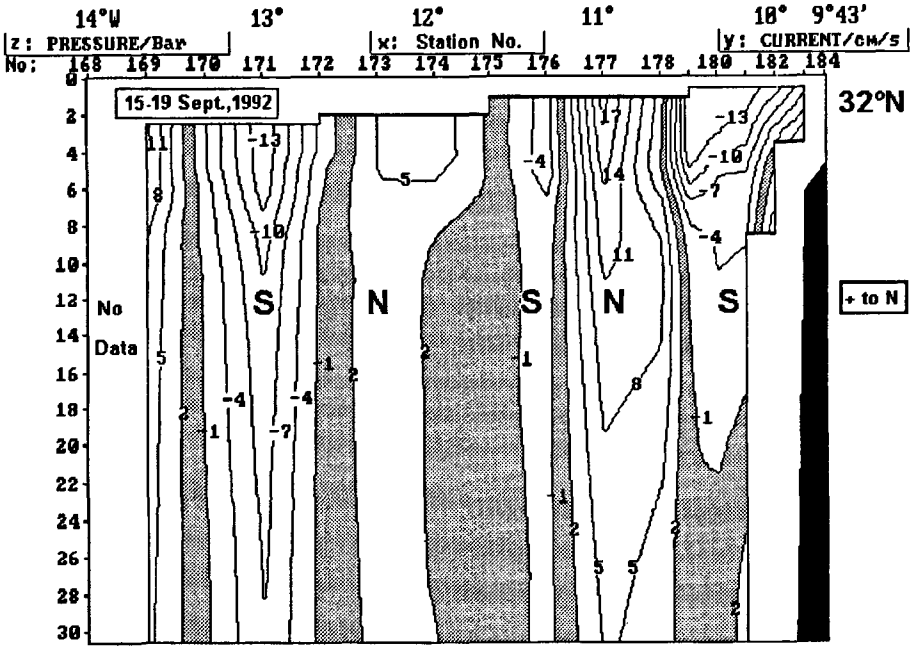

Obviously, smaller eddy-like features are present in this area, but there are unfortunately not sufficiently resolved by our station grid.

In order to inspect the current structures in greater detail, we also calculated the geostrophic currents relative to the "no-motion level" at 280 dbar along both zonal sections placed at 31° 30′ N and 30° 30′ N. Positive values indicate directions towards the north. There are two zonally well-separated cores of equatorward currents (–10 to –15 cm s^{-1}) with a distance of about 70 km not only in the north but also in the south (Fig. 15*a, b*). These current structures generally confirm the picture obtained from the relative dynamic topography in Figure 14*a*.

In addition, we calculated the net volume transport through a meridional section at 10° 10′ W and a section connecting stations 244 (31° 30′N, 11° 30′ W) and 252 (30° 30′ N, 11° 10′ W), in order to obtain a rough estimation of the mass balance within the 300 dbar top layer. Here, positive transports are in a westward direction. Thus, a closed box is formed (Fig. 2). Its western border encloses the angle of –15° from North and is aligned with the main wind direction NNE. The mean alongshore component of the wind stress is –0.06 N m^{-2}, corresponding to the velocity of 6 m s^{-1}. The resulting Ekman offshore transport is about –0.06 Sv (1Sv = 10^6 m^3 s^{-1}) between both zonal sections. Along the shelf edge, the geostrophic onshore transport is 0.04 Sv between both zonal sections (Fig. 15*c*). In other words, the Ekman offshore transport in the upper layer is nearly compensated by the geostrophic onshore transport within the 110 m subsurface layer. Considering the box, the inflow is given by –0.52 Sv from the north (stations 32-44), while the outflow is –0.21 Sv through the southern section (stations 285-297) but 0.59 Sv through the western section (stations 244-252) as plotted in Figure 15*d*. The leakage is 0.28 Sv. This deficit should be compensated by

Figure 13

T-S diagrams from three selected stations indicating the correspondence of water properties in intermediate layers with T < 15 °C and S < 36.1 between stations 180 (core of the southward coastal jet at 32° N) and 239 (offshore extension of the Gape Ghir filament with SST > 20 °C); significantly different water properties occur at station 264 (near coastal area of the cold water filament with SST < 20 °C above the southeastern flank of the Cape Ghir Plateau); station positions are shown in Figure 2.

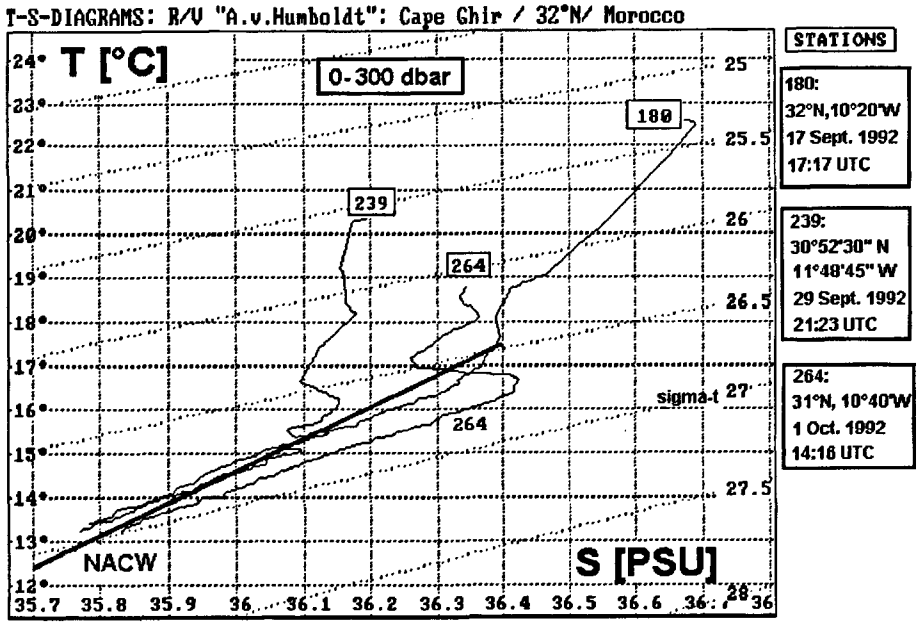

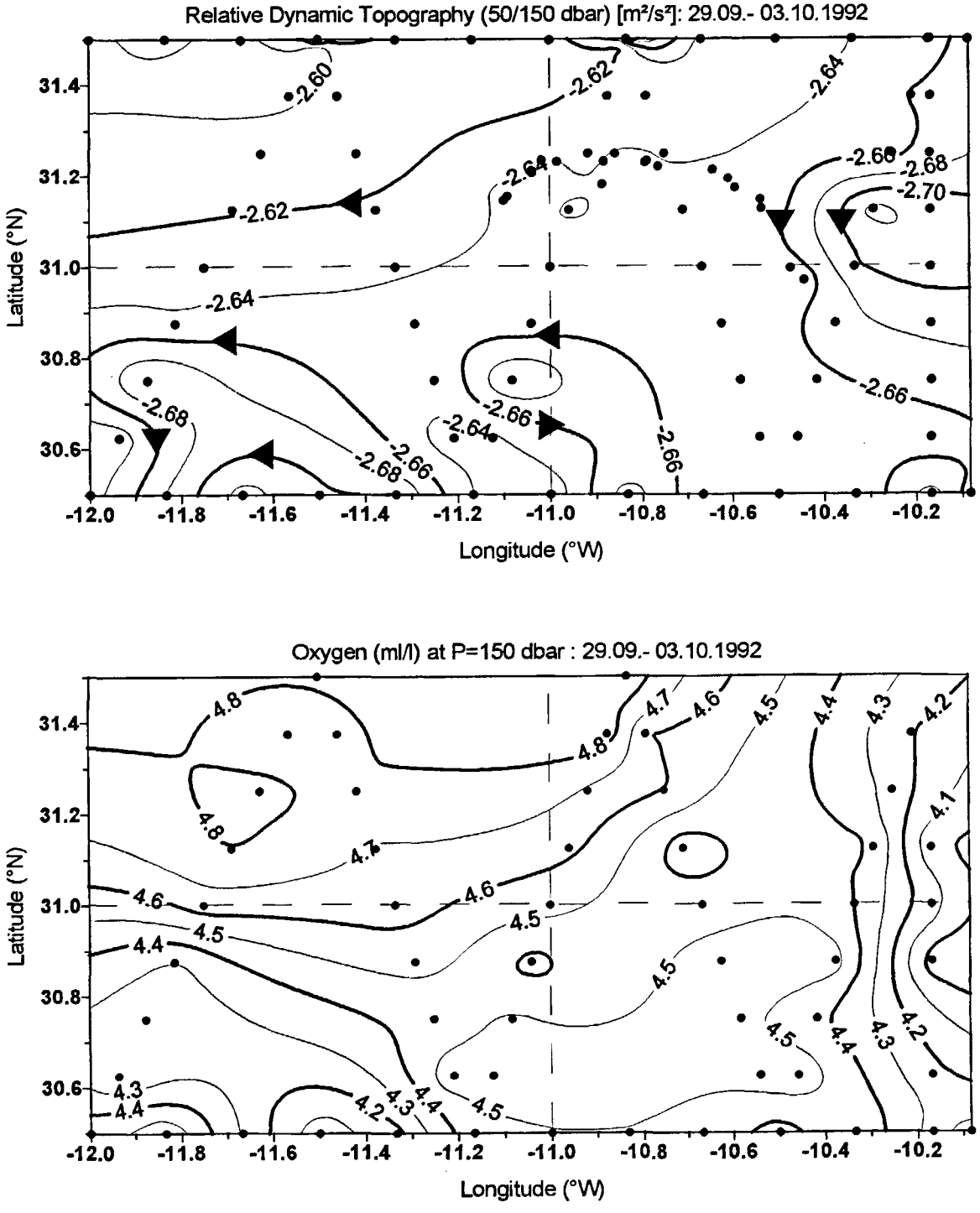

Figure 14

Spatial structures in the superficial mass field above the Cape Ghir Plateau and station positions (dots):
a) Dynamic topography at 50 dbar relative to 150 dbar; the smaller the distance between neighbouring isolines, the stronger the geostrophic current velocity with higher values on the right-hand side of the downstream direction.
b) Structures in the dissolved oxygen (O_2) at the pressure level of 150 dbar.

upwelling. The upwelling region is nearly located between the coast and 11° W where the course of the 20 °C isotherm marks the western border of the filament in Figure 7*a*. The upwelling domain could be considered as situated between (11° – 10° 10') W and (31° 30' – 30° 30') N, an area of about 80 km x 95 km = 7600 km^2. These values suggest the spatially averaged vertical velocity to be 3.7 x 10^{-3} cm s^{-1}, a typical value for the northwest African coastal upwelling areas (Hagen, 1976).

For the westward branch of the coastal jet, we note a core speed of 26 cm s^{-1} between stations 247 and 248 in Figure 15*d*. Comparing this value with that of –10 cm s^{-1} in the offshore branch in Figure 15*a*, the speed in the fila-

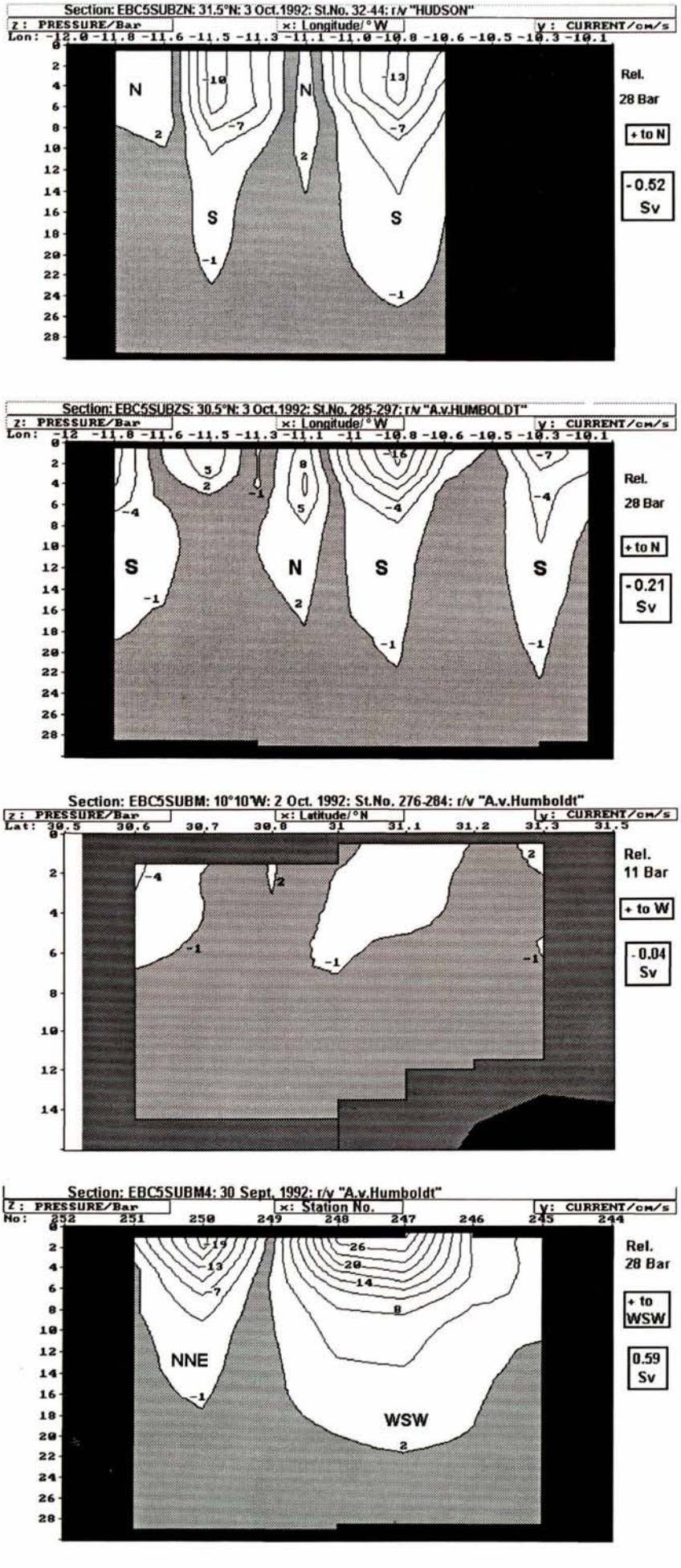

Figure 15

Geostrophic current structures along transects of the Eastern Boundary Current programme (EBC) forming a box for the estimation of the net balance of volume transports (1 Sv = 10^6 m^3 s^{-1}) in the 300 dbar top layer; sections are shown in Figure 2:

a) Along the northern border (EBC5SUBZN) at 31° 30' N, positive values relate to northward currents (N) relative to the 28 Bar (≈ 280 m) reference level;

b) As in Figure 15a but along the southern border (EBC5SUBZS) at 30° 30' N;

c) Along the eastern border (EBC5SUBM) at 10°10' W; positive values relate to westward flowing currents (W) relative to the 11 Bar (~110 m) reference level;

d) As in Figure 15a, b but along the western border (EBC5SUBM4); positive values relate to currents headed west-southwest (WSW).

ment current roughly increases by a factor of 2-3 along the frontal zone. Therefore, the offshore branch encloses a stronger core velocity than the onshore branch in Figure 15*b*. This acceleration suggests that there is another driving force in the filament current. Its large offshore extension could be supported by the two detected eddies propelling water seawards on both sides of the frontal zone.

Hydrographic structures

Vertical temperature, salinity, and potential density distributions along both zonal sections are plotted in Figure 16*a*, *b*, *c*. Oxygen measurements are only available from the southern section. Results are plotted in Figure 17. The two Figures reveal the following:

– The 20 °C isotherm, which roughly indicates the offshore position of the near-surface frontal zone, intersects the sea surface at 10° 25′ W in the north but at 10° 40′ W in the south.

– Within the frontal zone, zonal gradients in temperature are somewhat stronger in the north.

– The zonal extension of the near-surface frontal zone is about 50 km at 31° 30′ N but about 80 km at 30° 30′ N.

– Seaward of the near-surface frontal zone, the isotherms are located at greater depths in the north.

– The thermocline only coincides with a pronounced halocline along the northern section. There is no clear evidence of any inclination of the halocline along the southern section.

– Off the continental slope, relatively homogeneous conditions of salinity are found within the layer between 80 m and 140 m in the north but from the sea surface down to a depth of about 100 m in the south.

– The different zonal temperature and salinity structures are vertically compensated with respect to the potential density.

– The outcropping of the 26.2 kg m^{-3} isopycnal suggests a smaller zone of shelf break upwelling in the north than in the south.

– The thickness of the well-mixed top layer, which is bounded by the isopycnal of 25.6 kg m^{-3}, is about 50 m in the north but 30 m in the south.

– A relative maximum in dissolved oxygen is detected in the pycnocline, which is located between 30-60 m depth.

Comparing Figure 17 with Figure 15*b*, the relative minimum of dissolved oxygen (O_2 < 4.2 ml l^{-1}), which is visible at depths below 120 m between 11° 20′ W and 11° 30′ W, is coupled with poleward currents above the deep canyon in the bottom topography. Hydrographic structures in the cold-water belt following the shelf edge can be described by the section connecting stations 276 and 284 along

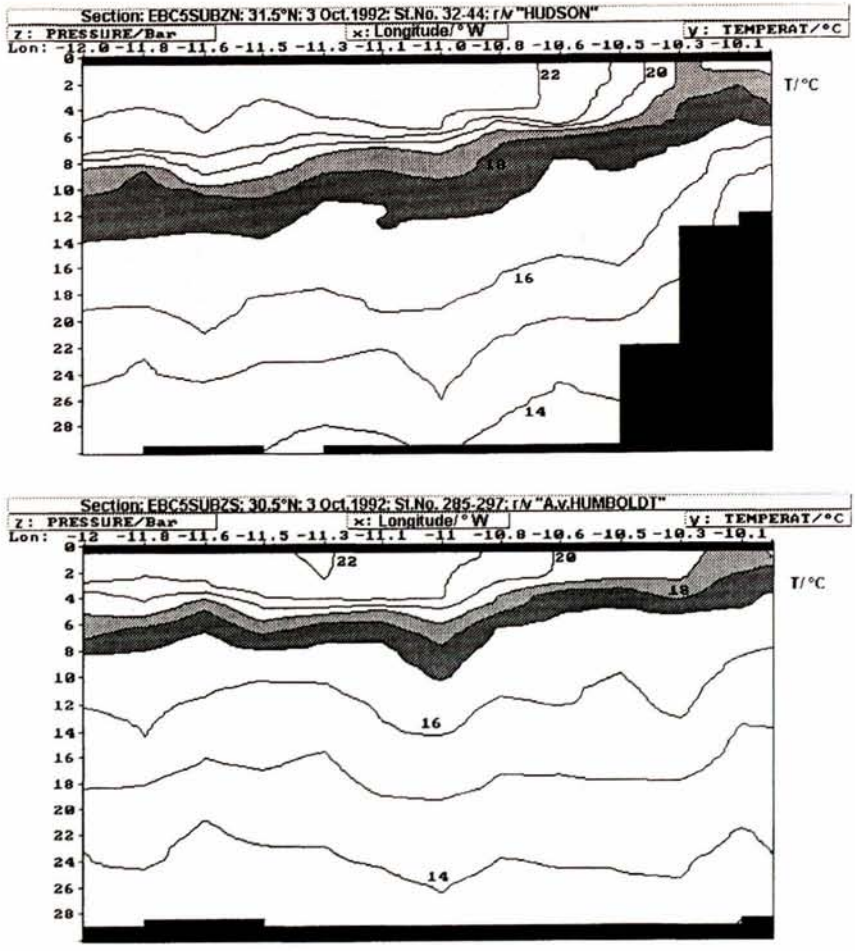

(a)

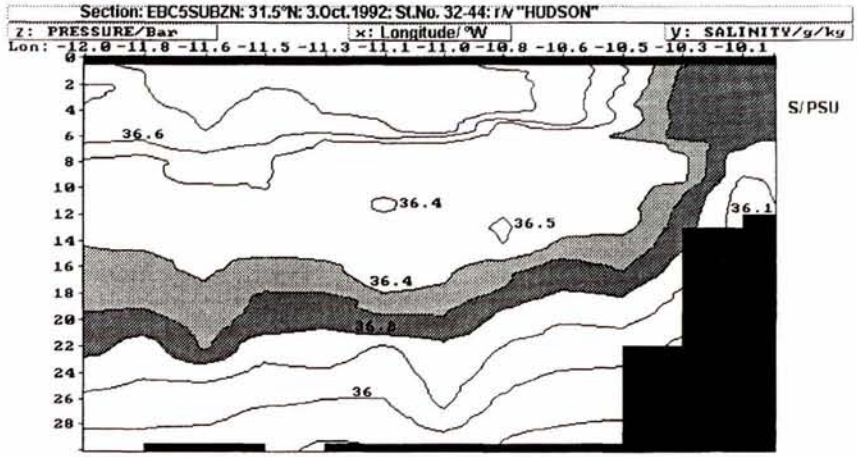

(b)

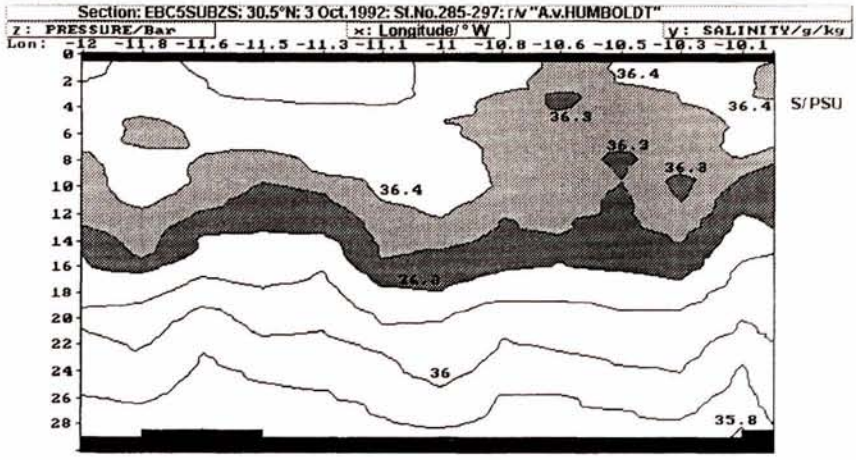

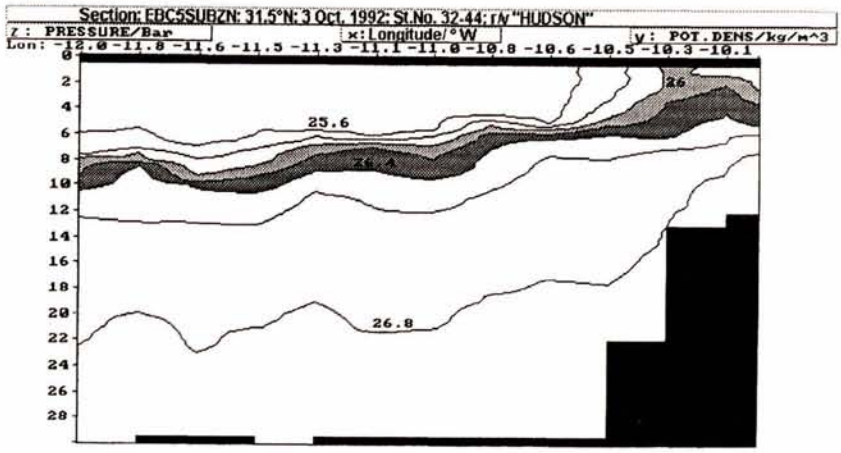

(c)

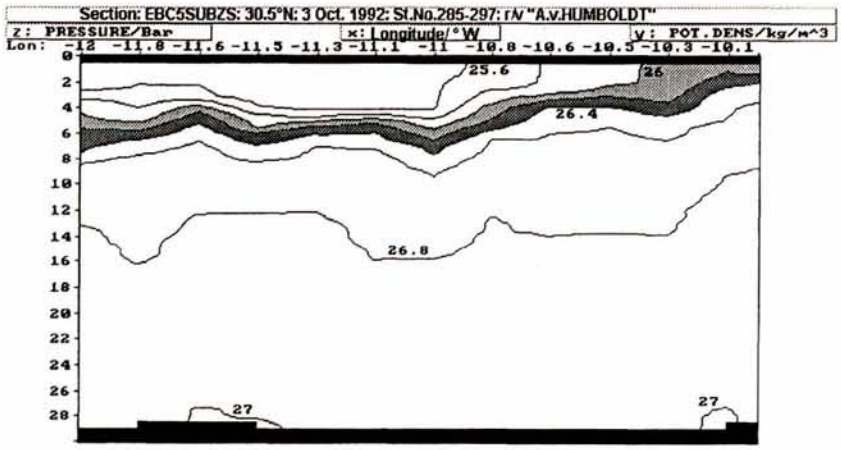

Figure 16

← *a*

b, *c* →

Vertical structures (Bar) along the zonal sections both in the north and in the south of the CGP:
a) Temperature (T °C); the thermocline between 17-19 °C is hatched;
b) Salinity (S); the layer between 36.2-36.4. is hatched;
c) Potential density (PD[kg m^{-3}]); the pycnocline between (1026 [26.0]-1026.4 [26.4]) kg m^{-3} is hatched.

10° 10′ W. Water depths lie in between 100 m and 750 m. The shallowest region occurs in the north, due to the crest of the CGP. For example, the temperature distribution is drawn in Figure 18. There is a clear inclination of the 16 °C-isotherm starting at about 120 m depth in the southern corner and ending at about 50 m depth in the north. The meridional gradients of temperature disappear above the CGP. Both the salinity isoline of 36.2 and the dissolved oxygen reading of 4.5 ml l^{-1} roughly coincide with the course of the 16 °C isotherm. This circumstance also suggests that active upwelling occurs more intensively in the northern part of this section (*cf.* Fig. 7*a*). The westernmost extension of the cold-water tongue was identified in the SST at 30° 50′ N, just along the southern flank of the CGP. In addition, our station grid provides a zonal transect along 31° N. The resulting temperature plot is shown in Figure 19. The isotherm of 20 °C intersects the sea surface at 11° 10′ W or, in other words, 50-70 km further to the west than along the southern and northern section.

Moreover, there is no indication here of a well-mixed top layer. Zonal gradients in temperature are to be found over the whole 300 dbar top layer east of station 240 (11° 45′ W). The layer, which is bounded by the isotherms of 15 °C and 16 °C, is inclined from about 170 m depth in the west to 110 m in the east. The corresponding plots of salinity, dissolved oxygen and potential density generally confirm such a zonal inclination. Furthermore, the layer with the relative maximum in oxygen ($O_2 > 5.1$ ml l^{-1})

gences in the entire water column to feed the cold-water filament.

Current response to such topographic obstacles has, for instance, been studied off Vancouver Island by Ikeda *et al.* (1984) using a nonlinear model. Filament formation mechanisms are suggested as being related to changes in the vertical current profile due to alongshore variations in the bottom topography. Baroclinic instability, which is caused by the shear between southward-flowing currents (coastal jet) in the upper layer and northward motions in deeper layers (undercurrent), could be one of the dominant mechanisms forming such filaments. The energy for large filaments was mainly provided by complicated nonlinear interactions including the modulation of shorter filaments. The nonlinear interactions were, however, mostly barotropic. Further, coastal upwelling and eddy development have been investigated off Nova Scotia by Petrie *et al.* (1987). Length and time scales of observed features were consistent with results from linear instability models. Their findings support the hypothesis that eddy-like features seen in infrared imagery were primarily due to the instability of the wind-driven coastal jet. They concluded that wind-driven coastal upwelling and subsequent baroclinic instability with eddy formation are probably quite important, but there is also some evidence that such filaments are related to barotropic instabilities of the surface jet associated with the upwelling over the shelf. Not only the [illegible] ment-filament interaction but also such barotropic current

Figure 18

Temperature distribution along the meridional section (EBC5SUBM) at 10° 10′ W through the coastal upwelling belt on the shelf; the thermocline between 16-17 °C is hatched.

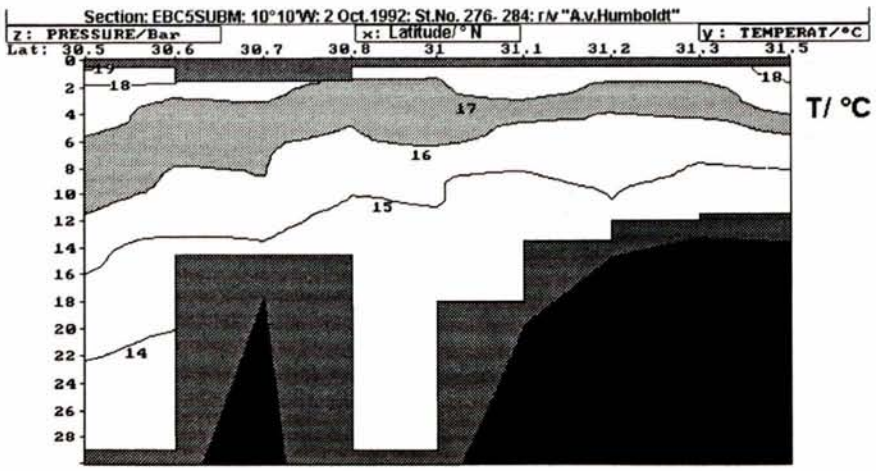

plateau. The shelf width and the radius of deformation are, according to Pedlosky (1979), coupled by the dimensionless stratification parameter $S = R^2/L^2$. The lower the value of S, the stronger the tendency to a generation of baroclinic instabilities in the motion field. For similar values of R, this tendency increases with increasing L. Thus, we obtain $S_P = R^2/L_P^2 = 0.032$ and $S_S = R^2/L_S = 0.114$. The resulting ratio S_S/S_P shows a factor of about 4. The smaller amount of S_P suggests that such instabilities are more probable over the CGP. At present, current measurements are not available from the Cape Ghir region. We expect characteristic on-offshore and alongshore currents in the same range as those observed by Mittelstaedt *et al.* (1975) at 21° 40′ N. The offshore current (U) exhibits core speeds of about 10 cm s^{-1}, while that of the coastal jet (V) is about 20-25 cm s^{-1} in near-surface layers. The poleward undercurrent is a characteristic ingredient of coastal upwelling processes off northwest Africa (Barton, 1989). Its core velocity is about 10 cm s^{-1} within intermediate layers. According to Tomczak (1989), there is also some observational evidence for its vertical migration in response to the seasonal southward progression of the upwelling.

Considering on-offshore motions, the residence time can be estimated by T = L/U to be 17.4 days over the CGP but 9.2 days in the coastal upwelling region. There is a factor of about 2. For the same time of residence, the core speed in the seaward-headed filament jet should be twice that of offshore motions of large-scale upwelling regions.

The local Coriolis frequency is $f = 7.51 \times 10^{-5}$ s^{-1} at the latitude of 31° N. Using the mean radius of deformation R = 27 km for the current width and V = 20 cm s^{-1} for the core speed of the coastal jet, we estimate the Rossby number $Ro = \xi / f \approx V/(Rf) \approx 0.1$. Here $\xi \approx V/R$ is a rough estimation for the associated relative vorticity. The resulting value suggests a comparatively large production of relative vorticity. In other words, we may expect an essential contribution of nonlinear dynamics in the maintenance of the filament. Usually, the influence of nonlinear motion dynamics can be only neglected for $Ro << 1$. Such dynamics also determine the mass-field structures in superficial layers and at the sea surface.

Mapped sea-surface temperatures (SST) provided by satellites and bulk SSTs from CTD measurements show a strict correspondence. Both reflect the response of the mass- and geostrophic current field to the bottom topography. This result confirms the conclusion of Holladay and O'Brien (1975) that daily SST fields respond rapidly to the local wind forcing but that isotherms of decadal SST maps tend to follow the large-scale bathymetry. Our results of the

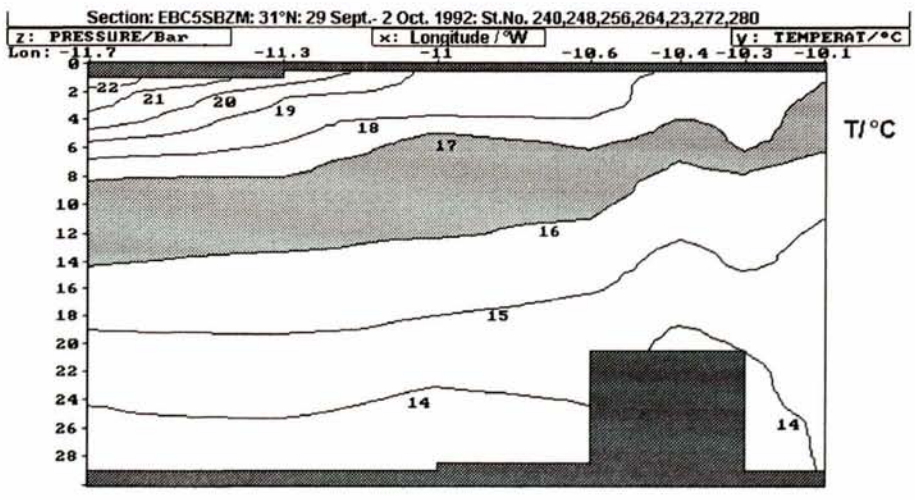

Figure 19

Temperature distribution along the zonal section (EBC5SBZM) at 31° N; the thermocline between 16-17 °C is hatched.

superficial structure of geostrophic currents are schematically summarized in Figure 20. This sketch is mainly based on the map of the relative dynamic topography shown in Figure 14*a*. Related hydrographic observations were carried out by means of a two-ship field campaign over the Cape Ghir Plateau between 30° 30′ N and 31° 30′ N, 10° 05′ W and 12° W in September-October, 1992.

The field measurements started after a relaxation phase in the large-scale upwelling process, which should be related to the seasonal southward migration of the north east trade in early autumn. Active coastal upwelling is only detected on the shelf, in a near-coastal strip bounded by the 150-300 m isobath. At 32° N, the equatorward coastal jet indicates geostrophic core velocities of about 13 cm s^{-1} within the 50 m top layer. Hypothetically, the filament could also be forced by this coastal jet flowing over decreasing water depths on its way to lower latitudes. Because the coastal jet is related to the large-scale upwelling, the generation of the filament could be relatively independent of local wind conditions. Its current core follows the continental slope to bifurcate into two branches over the northern flank of the CGP. One branch, trapped along the shelf edge between 150-300 m depth, is identified with the coastal/frontal jet itself. Its zonal width is about 15-25 km and coincides well with the scale of the first-mode radius of deformation. This branch transports the upstream water properties across the CGP southward, while the offshore branch meanders out to the west to form the cold-water filament over the CGP. In the filament, water properties of the coastal upwelling are zonally transported further offshore, up to distances of about 200 km from the coastline. The filament axis follows 30° 50′ N. Its geostrophic current core is embedded in a surface frontal zone separating the cold upwelling water, which dominates over the CGP, from the warm offshore water.

Several field studies carried out off California support the hypothesis that the jet, which follows the rim of the filament, is a branch of the southward "coastal jet". Due to the influence of the CGP on the downstream dynamics via nonlinear interactions between the barotropic mode and baroclinic modes, the frontal zone and the coastal jet form a large offshore meander generating a cyclonic, eddy-like feature above the topographic plateau. Such a direction of rotation locally supports upward vertical velocities (Defant, 1961). Related biological processes are discussed, for instance, in Angel and Fasham (1983).

In addition, our measurements indicate two oppositely rotating eddies. Looking in the upstream direction of the frontal jet, the cyclonic eddy is located on the cold-water side (southern flank of the CGP), while the anticyclonic eddy lies on the warm-water side (northern flank of the CGP). According to observations by Mooers and Robinson (1984), there is some evidence that pairs of oppositely-rotating eddies interact to generate an intense jet and to export cold coastal upwelled water out to sea. Such motion structures can be understood by the response of southward-moving currents over a submarine plateau by highly nonlinear interaction mechanisms between the barotropic mode and the sum of several baroclinic modes. Considering the simple barotropic case, the background potential vorticity f/H_0 could be balanced by $(\xi + f)/H$ due to the vorticity conservation along a stream line. The undisturbed water depth is H_0 while the topographic anomaly relative to the actual depth H is $h = H\text{-}H_0$. Thus we obtain $Ro = h/H_0$. From $H_0 = 2000$ m to $H = 1800$ m we get again $Ro = 0.1$. Along the northern flank of the CGP, we find $h = (H\text{-}H_0) < 0$ but over its southern flank $h > 0$. Consequently, there must be also a barotropic tendency for the generation of anticyclonic eddies with $\xi < 0$ in the North but for cyclonic eddies with $\xi > 0$ in the South of the CGP. We assume that such tendencies strictly influence the baroclinic motion field via nonlinear interaction mechanisms.

Simple transport estimations support the conclusion that active upwelling processes occur in the filament. These vertical velocities must be of the same order as in usual upwelling areas. Due to technical restrictions, our CTD measurements were carried out only within the 300 dbar

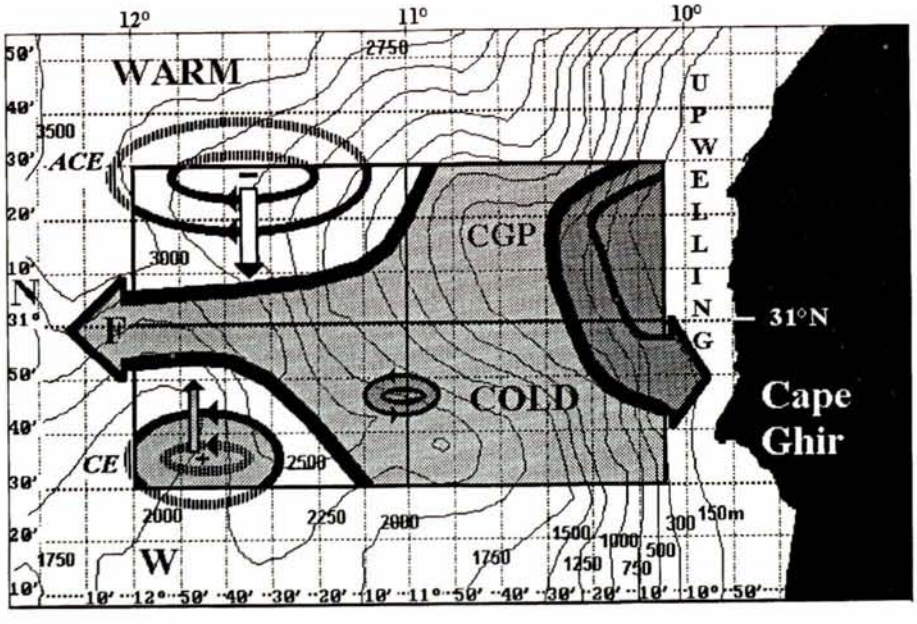

Figure 20

Area of investigation (box) with the sketch for detected (full line) and fictive (broken line) patterns of geostrophic motions within superficial layers; arrows indicate the cyclonic course of the southward coastal jet and the westward filament current (F) over the rough bottom topography of the Cape Ghir Plateau (CGP); isobaths in metres; shaded areas indicate cold water zones with an active upwelling centre in the northeast corner; two oppositely rotating eddies propel upwelled water out to the open Atlantic along the filament axis at about 31° N; in addition the cyclonic eddy (CE) generates upward-directed vertical velocities (+) while the anticyclonic eddy (ACE) produces downward vertical velocities (–); data are based on CTD measurements between 29 September and 3 October, 1992.

top layer. Unfortunately, our data base cannot provide any dynamic explanations concerning interaction processes between the mass- and current field and the CGP. The only aim of this note was to furnish a detailed description of actual mass field structures within the upper layers of the Cape Ghir filament.

In order to obtain more insight into the filament dynamics, numerical simulations of changes in different forcing conditions are in preparation. Possible candidates are changes in large-scale winds as well as both the strength of the coastal jet in near-surface layers and the poleward undercurrent occurring in deeper layers.

Acknowledgements

Measurements on board R/V *A. v.Humboldt* were financially supported by the Bundesminister für Forschung und Technologie in the framework of the German contribution to WOCE, contract 03F0050G/H and the EU Human Capital and Mobility Programme, contract ERBCHRXCT 930312; we wish to express our gratitude to Dr Harrison for timely submission of the CTD data of R/V *Hudson*; our thanks also to the reviewers for critical and constructive comments, as well as to Drs E. Mittelstaedt and P. Schlittenhardt for suggestions and fruitful discussions.

REFERENCES

Allen J.S. (1980). Models of wind-driven currents on the continental shelf. *Ann. Rev. Fluid Mechanic* **12**, 389-433.

Angel M.V., M.J.R. Fasham (1983). Eddies and biological processes. *In:* Eddies in Marine Science, ed. A.R. Robinson, Springer-Verlag, 492-524.

Barton E.D. (1989). The poleward undercurrent on the eastern boundary of the subtropical North Atlantic. *In*: Poleward Flows Along Eastern Ocean Boundaries, Coastal and Estuarine Studies, 34, eds. Neshyba S.J., C.N.K. Mooers, R.L. Smith, R.T. Barber, Springer Verlag, 82-92.

Brink K.H. (1983). The near-surface dynamics of coastal upwelling. *Progress in Oceanography* **12**, 223-257.

Defant A. (1961). Water bodies and stationary current conditions at boundary surfaces. *In*: Physical Oceanography, Vol.1, Pergamon Press, 451-475.

Emery W.J., W.G. Lee, L. Magaard (1984). Geographic and seasonal distribution of Brunt-Väisälä frequency and Rossby radii in the North Pacific and North Atlantic. *Journal of Physical Oceanography* **14**, 294-317.

Erimesco P. (1966). Observations à propos de l'hydrologie de l'océan Atlantique au large des côtes du Maroc. *Bulletin de L'Institut des Pêches Maritimes du Maroc* **14**, 8-28.

Fiekas V., J. Elken, T.J. Müller, A. Aitsam, W. Zenk (1992). A view of the Canary Basin thermocline circulation in winter. *Journal of Geophysical Research* **97**, 12495-12510.

Gabric A.J., L. Garcia, L. Van Camp, L. Nykjaer, W. Eifler, W. Schrimpf (1993). Offshore export of shelf production in the Cape Blanc (Mauritania) giant filament as derived from Coastal Zone Colour Scanner imagery. *Journal of Geophysical Research* **98**, 4697-4712.

Hagen E. (1976). Ein Beitrag zur Erkundung des Kaltwasserauftriebs vor Nordwestafrika, speziell für das Schelfgebiet vor Cap Blanc. *Beiträge zur Meereskunde* **37**, 29-72.

Hagen E., E. Mittelstaedt, R. Feistel, H. Klein (1994). Hydrographische Untersuchungen im Ostrandstromsystem vor Portugal und Marokko 1991-1992. Berichte des Bundesamtes für Seeschiffahrt und Hydrographie, Nr. 2, 49 p.

Halpern D., D. Stuart (1975). On near-surface wind observations: Part 4. Preliminary JOINT-I results: Buoy Lisa, buoy Michael and coastal stations Eight and Nine wind measurements. CUEA-Newsletter, **4**, 17-23.

Head E.J.H., W.G. Harrison, B.I. Irwin, E.P.W. Horne, W.K.W. Li (1995). Plankton dynamics in an area of upwelling off the coast of Morocco. *Deep Sea Research* (submitted).

Holladay C.G., J.J. O'Brien (1975). Mesoscale variability of sea surface temperatures. *Journal of Physical Oceanography* **5**, 761-772.

Ikeda M., W.J. Emery, L.A. Mysak (1984). Seasonal variability in meanders of the California current system off Vancouver Island. *Journal of Geophysical Research* **89**, 3487-3505.

Ikeda M., W.J. Emery (1984). A continental shelf upwelling event off Vancouver Island as revealed by satellite infrared imagery. *Journal of Marine Research* **42**, 303-317.

Ismer H.J., L. Hasse (1987). The Bunker Climate Atlas of the North Atlantic Ocean, Vol. 2: Air-Sea Interaction. Springer-Verlag, 252 p.

Kirk A., P.Speth (1985). Wind conditions along the coast of Northwest Africa and Portugal during 1972-79. *Tropical Ocean-Atmosphere Newsletter* **30**, 15-16.

Kosro P.M., A. Huyer (1986). CTD and velocity surveys of seaward jets off northern California, July 1981 and 1982. *Journal of Geophysical Research* **91**, 7680-7690.

Kosro P.M. (1987). Structure of the coastal current field off northern California during the coastal ocean dynamics experiment. *Journal of Geophysical Research* **92**, 1637-1654.

Kosro P.M., A. Huyer, S.R. Ramp, R.L. Smith, F.P. Chavez, T.J. Cowles, M.R. Abbott, P.T. Strub, R.T. Barber, P. Jessen, L.F. Small (1991). The structure of the transition zone between coastal waters and the open ocean off northern California, Winter and Spring 1987. *Journal of Geophysical Research* **96**, 14707-14730.

Lutjeharms J.R.E., P.L. Stockton (1987). Kinematics of the upwelling front off southern Africa. *South African Journal of Marine Science* **5**, 35-49.

Metzner M., I. Hennings (1990). Comparison of radar altimeter and AVHRR data of a coastal upwelling feature with first results of a circulation model. *In*: Proceedings of the Second Conference on "Ocean From Space", Venice, Italy, May 22-26, 1990, 4 p.

Mittelstaedt E., D. Pillsbury, R.L. Smith (1975). Flow patterns in the northwest African upwelling area. *Deutsche Hydrographische Zeitschrift* **28**, 145-167.

Möckel F. (1980). Die ozeanologische Meßkette OM 75, eine universelle Datenerfassungsanlage für Forschungsschiffe. *Beiträge zur Meereskunde* **43**, 5-14.

Mooers C.N.K., A.R. Robinson (1984). Turbulent jets and eddies in the California Current and inferred cross-shore transports. *Science* **223**, 51-53.

Nykjaer L., M. Metzner, P. Schlittenhardt, L. Van Camp (1987). Remote sensing of the Northwest African upwelling area. An example of the distribution of chlorophyll-like pigment and sea surface temperature. *In:* Proceedings of IGARSS'87 Symposium "Remote Sensing: Understanding the Earth as a System", University of Michigan May 18-21, 1987, 1595-1599.

Petrie B., B.J. Topliss, D.G. Wright (1987). Coastal upwelling and eddy development off Nova Scotia. *Journal of Geophysical Research* **29**, 12979- 12991.

Pedlosky J. (1979). Geophysical fluid dynamics. Springer-Verlag, New York, 624 p.

Rienecker M.M., C.N.K. Mooers (1988). Mesoscale variability in current meter measurements in the California current system off northern California. *Journal of Geophysical Research* **93**, 6711- 6734.

Schlüssel P., H.Y. Shin, W.J. Emery, H. Grassl (1987). Comparison with satellite-derived sea surface temperatures with *in-situ* measurements. *Journal of Geophysical Research* **92**, 2859-2874.

Siedler G., A. Kuhl, W. Zenk (1987). The Madeira mode water. *Journal of Physical Oceanography* **17**, 1561-1570.

Smith R.L. (1995). On the process of upwelling: New observations and understanding. *In*: Dynamics of Upwelling in the ICES Area, eds. E. Hagen and A.J. da Silva: ICES Cooperative Research Report **206**, 15-33.

Speth P., A. Köhne (1983). The relationship between sea surface temperatures and winds off Northwest Africa and Portugal. *Océanographie Tropicale* **18**, 69-80.

Tomczak M. (1989). Review and commentary to paper "The Poleward Undercurrent on the Eastern Boundary of the Subtropical North Atlantic", by E.D. Barton. *In:* Poleward Flows Along Eastern Ocean Boundaries, eds. S.J. Neshyba, C.N.K. Mooers, R.L. Smith, R.T. Barber, Coastal and Estuarine Studies, 34, Springer-Verlag, 93-95.

Thomson R.E., W.J. Emery (1986). The Haida current. *Journal of Geophysical Research* **91**, 845-861.

UNESCO (1987*a*). GF3 A general formatting system for geo-referenced data. *Manuals and Guides* **17**, 2. Technical Description of the GF3 Format and Code Tables. 1-42.

UNESCO (1987*b*). International Oceanographic Tables, Vol. 4, Properties derived from the International Equation of State of Seawater, 1980, *Technical Papers in Marine Science* **40**, 195 p.

Willenbrink E. (1982). Analysis of watermasses in the tropical and subtropical North-East Atlantic. *Berichte aus dem Institut für Meereskunde Kiel* **96**, 1-72.

Wooster W.S., A. Bakun, D.R. McLain (1976). The seasonal upwelling cycle along the eastern boundary of the North Atlantic. *Journal of Marine Research* **34**, 131-141.

Zülicke C. (1994*a*). AVHRR-HRPT SST scenes for AMOR-92: TeraScan products for 05.09.-05.10.92/30-45 N/4-16 W, Quick Look Tables. CEC/ JRC Ispra/ IRSA: Technical Note No. I. 94. 123, p. 8.

Zülicke C. (1994*b*). AMOR 92-scientific report: Atlantic measurements of oceanic radiation 1992 CEC/JRC Ispra/IRSA: Technical Note No. I. 94. 06, p. 62.